POSTERIOR INTRAPARIETAL SULCUS ACTIVITY DURING A HEAD UNRESTRAINED, MEMORY GUIDED REACH TASK

Brando Sheldrick

A THESIS SUBMITTED TO THE FACULTY OF GRADUATE STUDIES IN PARTIAL FULFILLMENT OF THE REQUIREMENTS FOR THE DEGREE OF MASTER OF ARTS

PSYCHOLOGY
YORK UNIVERSITY
TORONTO, ONTARIO

JULY 2026

© Brando Sheldrick, 2026

ABSTRACT

The goal of this study was to investigate the effect of allocentric visual information on the activity of macaque posterior parietal neurons. Local field potentials (LFPs) were recorded from the intraparietal sulcus (IPS) of two female *Macaca Mulatta* monkeys (ML) trained to perform a memory-guided reach task. During no landmark (NL) trials, a target briefly flashed at a random location, and after a memory delay, the animal was cued to reach to the remembered target position. During stable landmark (SL) trials, a landmark surrounded the target for the duration of the task, while shifted landmark (ShL) trials were associated with a surreptitious landmark shift of 8° in one of 8 directions following the memory-delay. I observed modulations in LFP data during SL and ShL trials relative to NL trials, but not during SL trials relative to ShL trials, along with differences in LFP activity between IPS areas.

DEDICATION

This project is dedicated to my friends and family. Thank you for your unconditional love, support, and guidance.

ACKNOWLEDGEMENTS

I would like to begin by thanking my supervisor, Dr. Douglas Crawford. Working under his supervision has broadened my horizons as a growing neuroscientist, and his encouragement to present our work at both national and international conferences has provided me with learning opportunities that many could only wish for. Observing his tutelage of not just myself, but the rest of our lab has been incredibly inspiring, and represents a standard of leadership that I will always strive towards. I also thank my thesis advisor Dr. Jeff Schall for his expert feedback and time spent on edits and meetings.

I would like to extend my utmost gratitude to Dr. Hongying Wang, Dr. Verónica Nácher, and Jennifer Lin for their immense work in training the animals and collecting behavioural and electrophysiological data and allowing me to participate in data collection from the second animal. I also want to thank Dr. Xiaogang Yan for setting up the experimental task, as well as the entire Vivaria staff for all of their hard work.

Thank you to Saihong Sun for providing the statistical analysis pipeline. As I lack the coding ability for such an immense undertaking, your expertise in coding was critical to the success of this project, and to the ongoing success of many of my fellow lab members work. Additionally, I would like to express an incredible amount of gratitude to Ashkan Karimi, whose assistance with an endless amount of troubleshooting and further statistical analysis helped this project get over seemingly insurmountable roadblocks. Finally, thank you to the rest of my fellow lab members and colleagues, whose friendship, support, and guidance has been incredibly important.

TABLE OF CONTENTS

ABSTRACT ii
DEDICATION iii
ACKNOWLEDGEMENTS iv
TABLE OF CONTENTS v
LIST OF FIGURES vii
CHAPTER 1 GENERAL INTRODUCTION 1
1.1 Egocentric and Allocentric Reference Frames 2
1.2 The Two-Stream Hypothesis 4
1.3 The Macaque Posterior Parietal Cortex 7
1.4 Local Field Potentials Recorded from Macaques 11
1.5 Cue Conflict Studies in Humans 13
1.6 Cue Conflict Studies in Macaques 17
1.7 Specific Questions and Hypotheses 20
CHAPTER 2 POSTERIOR INTRAPARIETAL SULCUS ACTIVITY DURING A HEAD UNRESTRAINED, MEMORY GUIDED REACH TASK 23
2.0 Abstract 24
2.1 Introduction 25
2.2a Animals and Surgical Procedures 28
2.2b Experimental Setup 29
2.2c Experimental Paradigm 31
2.2d Data Acquisition 34
2.2e Data Analysis 35
2.2g Spectral Analysis 36
2.2h Statistical Analysis 37
2.4 Results 38
2.4a Oscillatory Dynamics during the Memory-Guided Reach Task 38
2.4b Frequency-Dependent Oscillatory Power in the Memory-Guided Task 41
2.4c Influence of Landmark on LFP Oscillations 46
2.4e Band Specific Power Analysis 53
2.5 Discussion 65
2.5a Behavioural Differences in our Three Tasks 67

2.5b LFP Modulations During Memory-Guided Reach 68
2.5c LFP Modulations Associated with Allocentric Visual Information 70
2.5d Stable Landmark Vs. Shifted Landmark Trials 72
2.5e Overall Differences Between LIP, MIP, and VIP 74
2.6 Conclusion 74
CHAPTER 3 GENERAL DISCUSSION 75
3.0 Discussion 75
3.1 Summary and Implications 76
3.2 Clinical Implications 76
3.3 Limitations 77
3.4 Future directions 79
REFERENCES 81
APPENDICES 94
Appendix A: Author Contributions 94

LIST OF FIGURES

Chapter 1

Figure 1. Egocentric and Allocentric Reference Frames. 3
Figure 2. The human dorsal and ventral visual streams. 5
Figure 3. Lateral view of the macaque intraparietal sulcus. 9
Figure 4. Allocentric weight transformation procedure. 15
Figure 5. Influence of landmark shift relative to initial target position on allocentric weight. 18
Figure 6. Gaze, head and touch endpoints, and 2-D gaze trajectories for both animals. 20

Chapter 2

Figure 7. Laboratory setup. 30
Figure 8. All the possible locations of the target and the landmark. 32
Figure 9. Experimental task and timing. 33
Figure 10. Chamber coordinates. 35
Figure 11. LFP oscillatory dynamics during the reaching task. 40
Figure 12. Significant modulations in LFP power relative to baseline across no landmark (NL) trials. 45
Figure 13. Significant modulations in LFP power during stable landmark trials relative to no landmark trials. 50
Figure 14. Significant modulations in LFP power during shifted landmark trials relative to no landmark trials. 53
Figure 15. LFP power decomposed into frequency bands. 56
Figure 16. Modulations in frequency-band activity between areas during target flash event. 58
Figure 17. Modulations in frequency-band activity between experimental conditions during target flash event. 59
Figure 18. Modulations in frequency-band activity between areas during hand onset event. 61

Figure 19. Modulations in frequency-band activity between experimental conditions during hand onset event. 62
Figure 20. Modulations in frequency-band activity between areas during hand touch event. 64
Figure 21. Modulations in frequency-band activity between experimental conditions during hand onset event. 65

CHAPTER 1 GENERAL INTRODUCTION

To navigate throughout environments and interact with objects we encounter in our day-to-day lives, mammals must integrate and transform somatosensory signals into appropriate motor commands. In the context of reaching behaviour, a large body of work has been extensively devoted to studying the posterior parietal cortex (PPC), an area that is composed of numerous visual and motor hubs, such as the intraparietal sulcus (IPS). The IPS encodes visual information in a predominantly egocentric manner, such that cells along this area encode the physical location of objects in a coordinate system relative to one's own body in space, and are largely invariant to the presence of visual landmarks. Previous work has demonstrated that frontal cortex structures, including the frontal and supplementary eye fields (FEF; SEF), integrate target and landmark information in their visual response (Bharmauria et al., 2020, 2021; Seo et al., 2023). However, similar experiments have yet to be performed in the macaque parietal cortex during naturalistic reaching behaviours. The purpose of this current study was to investigate the effect of egocentric and allocentric visual information on the activity of neurons along the IPS. As the IPS predominantly encodes visual information in an egocentric frame of reference, I was curious to investigate the effect that landmarks and landmark shifts had on the spectral activity of neurons in this area, and whether they responded to or were invariant to the presence of reliable and unreliable landmarks. To investigate this query, I trained two head-unrestrained female macaques to perform a memory-guided reach task in the dark, where they performed arm reaches to a target either with or without a visual landmark. During landmark trials, the monkey was either exposed to a stable (reliable) or shifted (unreliable) landmark.

1.1 Egocentric and Allocentric Reference Frames

Whether reaching for a nearby coffee cup, grasping a door handle, or shaking a hand, mammals must constantly coordinate their visual and motor systems to successfully execute goal-directed actions. Such behaviours are second-nature to us, but behind the scenes, these simple actions are put into motion by a series of complex spatial transformations that coordinate our vision with our effectors to smoothly and effortlessly interact with our environment (Fiehler & Karimpur, 2023). Egocentric, or body-centered reference frames encode spatial information in a subject-object manner, such that objects in the environment are represented relative to the location of one's own body in space; while allocentric, or world-centered reference frames encode spatial information in an object-object manner, by representing the location of objects in space relative to the location of other objects or entities in the same environment (Moraresku & Vlcek, 2020; Simons & Wang, 1998) (Figure 1). Allocentric landmarks help to stabilize visual target representations and improve motor performance in both humans and monkeys (Byrne and Crawford, 2010; Byrne, Cappadocia, and Crawford, 2010; Li et al., 2018; Musa et al., 2024; Lin et al., 2024).

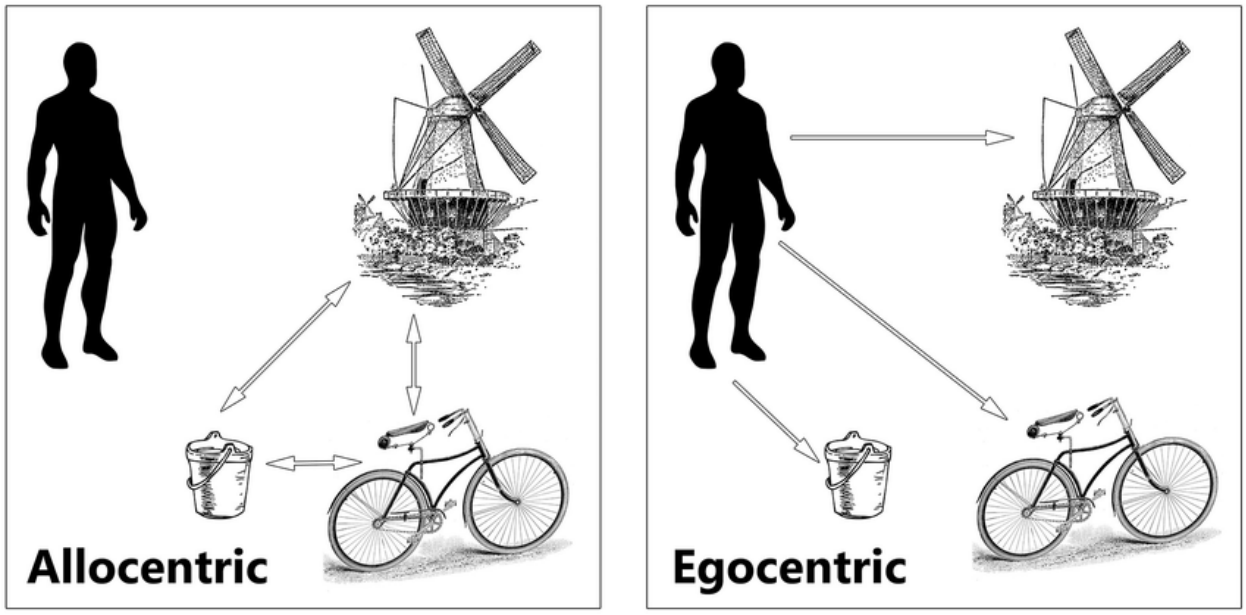

Figure 1. Egocentric and Allocentric Reference Frames. Allocentric reference frames encode spatial information about the location of a target in a coordinate system relative to other objects, or landmarks in space. Egocentric reference frames encode spatial information about the location of a target in a coordinate system relative to one's own position in space. Adapted from "Visual experience facilitates allocentric spatial representation.", by Pasquallotto, A., Spiller, MJ., Jansari, A., Proulx, M. *Behavioural Brain Research, 236, 175–179. https://doi.org/10.1016/j.bbr.2012.08.042*

Human neuroimaging studies have elucidated the cortical mechanisms underlying reach during egocentric and allocentric conditions, with egocentric visual information being primarily associated with activation in the parietofrontal network, and allocentric visual information being associated with greater recruitment of areas in the temporal and occipital cortices (i.e., inferior temporal gyrus and inferior occipital gyrus) (Chen et al., 2014). Macaque neuroimaging studies have observed similar cortical mechanisms associated with reaching behaviours under egocentric and allocentric conditions. For example, Neggers and colleagues (2006) reported that arm reaches associated with greater egocentric visual information primarily activate parietal areas, while reaches associated with greater allocentric visual information instead activate temporal areas.

Reach movements to a salient target are most accurate when egocentric cues are used in conjunction with allocentric information. Numerous studies have demonstrated that allocentric information can substantially influence reaching behaviours, and under many circumstances, is weighted more heavily than egocentric information during motor planning and execution (Bharmauria et al., 2024; Byrne & Crawford, 2010; Chen & Crawford, 2019; Lemay et al., 2004; refer to section 1.5 for further discussion).

1.2 The Two-Stream Hypothesis

Decades of neuropsychological and clinical evidence has supported the premise that the primate brain's visual system is divided along two streams: a dorsal stream, which projects from the striate cortex to the posterior parietal region (PPR); and a ventral stream, which projects from the striate cortex to the inferotemporal cortex (IT) (Figure 2) (Goodale & Milner, 1992; Goodale & Haffenden, 1998; Goodale, 2010; Milner & Goodale, 2007; Whitwell et al., 2014). Ungerleider & Mishkin (1982) suggested that visual processing of an object depended on the features that were being actively processed – for example, visual analysis of the qualities of an object (size, shape, semantic features) was processed throughout areas along the temporal cortex, while visual analysis of the physical location of the object in space was processed throughout areas along the parietal cortex. This functional segregation of a) object recognition, aesthetic judgements, and semantic meaning; and b) spatial awareness, motor planning, and action guidance along the respective ventral and dorsal sides of the mammalian brain has been further elaborated upon throughout the following decades. Neurons along the ventral, or "what" pathway represent the stable, physical characteristics of an object for the formation of persistent long-term representations, and rely more prominently on allocentric, over

egocentric visual information (Goodale & Haffenden, 1998). In contrast, neurons along the dorsal, or “where” pathway are associated with the visual guidance of goal-directed actions and online spatial processing for the physical manipulation of objects, and rely more prominently on egocentric, instead of allocentric visual information. The dorsal stream is associated with short-term, rather than long-term representations of objects, as egocentric representations often degrade <500 ms after a memorized object is occluded (Goodale & Haffenden, 1998; Westwood et al., 2001).

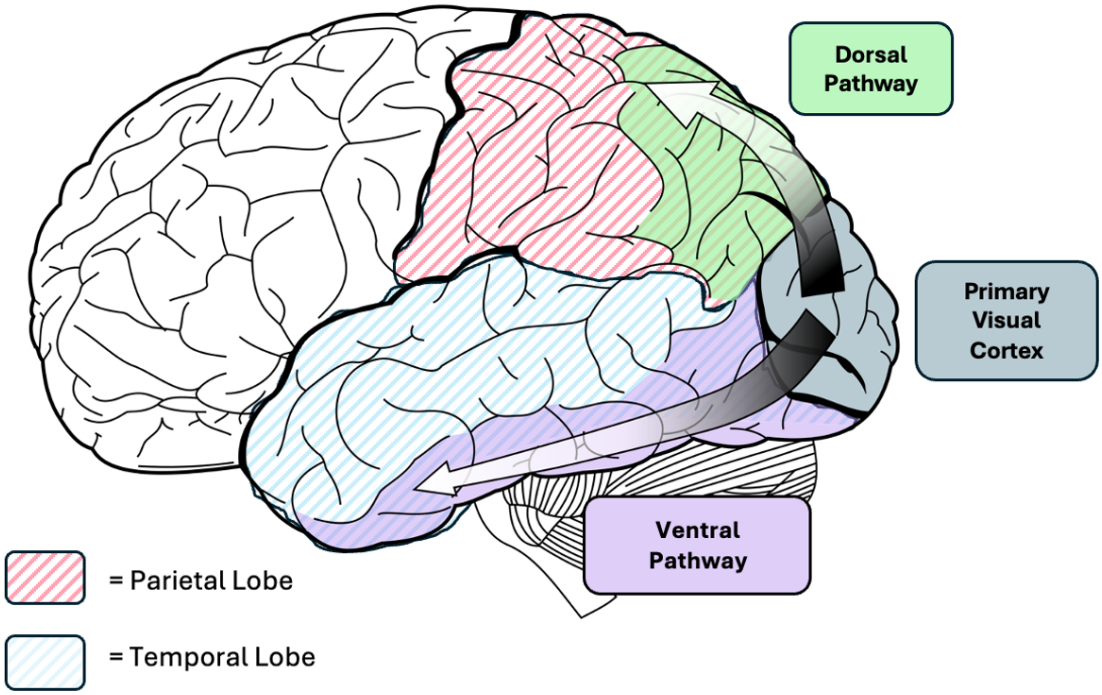

Figure 2. The human dorsal and ventral visual streams. Visual information is first processed in the primary visual cortex, before being segmented along the dorsal or ventral paths. The dorsal (or “where”) path, which runs from the striate region to the PRR is primarily responsible for encoding visual motion and properties associated with object interaction. The ventral (or “what” path, which runs from the striate region to the inferotemporal region is primarily responsible for object recognition, semantic meaning, and aesthetic qualities. Adapted from INPSYCH (2024). How do we see? https://in-psych.co.uk/2024/05/how-do-we-see/

Both neuroimaging and electrophysiology studies in macaques have supported the premise that two visual streams exist along the ventral and dorsal sides of the brain (Britten et al., 2009; Lafer-Sousa & Conway, 2013; Smith et al., 2005; Tsao et al., 2006; Wang et al., 2024). One fMRI study determined the presence of multiple specialized patches along the macaque ventral stream that are functionally divided to respond to the presence of colour, faces, and body parts, many of which were independently segregated and non-overlapping (Lafer-Sousa & Conway, 2013). Another study conducting single-unit recordings in macaque area MT (along the dorsal stream) reported that these cells responded most strongly to objects in motion and were largely invariant to the aesthetic features of objects (Smith et al., 2005).

Numerous studies have elucidated the neural mechanisms underlying reaching in both humans and primates (Batista et al., 1999; Connolly et al., 2000; Chen et al., 2014; Culham et al., 2003). In Chen et al.'s (2014) study, human participants reached to targets under egocentric and allocentric conditions while undergoing fMRI. Under egocentric conditions, Chen et al. (2014) reported an increased BOLD signal in areas along the dorsal visual stream (premotor cortex, medial intraparietal sulcus, and superior parieto-occipital cortex), while allocentric reaching conditions elicited a strong BOLD signal in early vision areas (lingual gyrus, inferior occipital gyrus, calcarine sulcus, and cuneus), as well as areas along the ventral visual stream (inferior temporal gyrus). However, fMRI studies suggest that allocentric information (perhaps from the ventral stream) is incorporated into the dorsal stream when landmark-centred actions are required (Chen et al. 2018, 2020).

1.3 The Macaque Posterior Parietal Cortex

The PPC has been well characterized as a region associated with guiding eye and arm movements towards intended targets and facilitating future reach plans (Andersen & Bueno, 2003; Batista et al., 1999; Buneo et al., 2002; De Vitis et al., 2019; Eskander & Assad, 1999; Fattori et al., 2005; Marzocchi et al., 2008; Snyder et al., 1997; Yttri et al. 2013). The PPC is composed of a number of important areas, including V6A, PE, parietal reach region (PRR), and the interparietal sulcus (IPS), all of which are highly involved in different aspects of visually- and memory-guided reaches and saccades towards targets.

Macaque parietal area V6A is located on the superior parietal lobule, and is populated with cells that are primarily responsive to the coordination of gaze and the perception of visual stimuli. Marzocchi et al. (2008) reported that monkeys performing reaching movements to a target in the dark displayed neural activity in area V6A that was modulated by the direction of the monkey's gaze during the reaching movement. Additionally, Fattori et al. (2005) observed that the activity of V6A neurons responded most strongly to outward and inward reaching movements, concluding that these neurons are involved in the process of coding the direction of an arm movement towards a target in space.

Macaque area PE shares many connections with premotor, motor, and sensory areas and is topographically organized, dominated by neural representations of the macaque hand, forelimb, shoulder, and leg (De Vitis et al., 2019). Additionally, area PE has been well-characterized as a site associated with motor preparatory signals, along with the generation of reaching movements in an egocentric coordinate system. The activity of the cells along the medial bank of PE is also tuned by both depth and direction

of reaching activity. De Vitis and colleagues (2019) exposed macaques to a visually-guided reach task, and observed that PE direction-tuning cells discharged most strongly after fixation on a target, but PE depth-tuning cells were most prevalent during the period where the animal moved its arm and interacted with the target.

The PRR composes a hub of areas, including portions of macaque V6A, along with the medial intraparietal sulcus. The PRR is considered an early hub in the visuomotor hierarchy, with neurons responding most strongly to the planning of an arm reach towards a target (Synder et al., 1997; Yttri et al., 2013). The macaque IPS is composed of numerous different sites, segregated along the medial (MIP), lateral (LIP), and ventral (VIP) banks (Figure 3). The MIP, along with neighbouring sites are part of the PRR network, and as such, is strongly associated with guiding arm and hand movements towards a target (Pesaran et al., 2006; Grefkes & Fink, 2005). Pesaran and colleagues (2006) reported that macaque MIP cells discharged in an eye-centred pattern as monkeys pointed to a target while maintaining visual fixation centrally, indicating that these cells respond primarily in egocentric, rather than allocentric coordinates. Furthermore, MIP cells fired strongly when monkeys used a joystick to direct a moving dot to a target location, but did not fire when monkeys observed a recorded video of the task, suggesting that these neurons respond strongly to the coordination of hand movements with visual targets (Eskander & Assad, 1999).

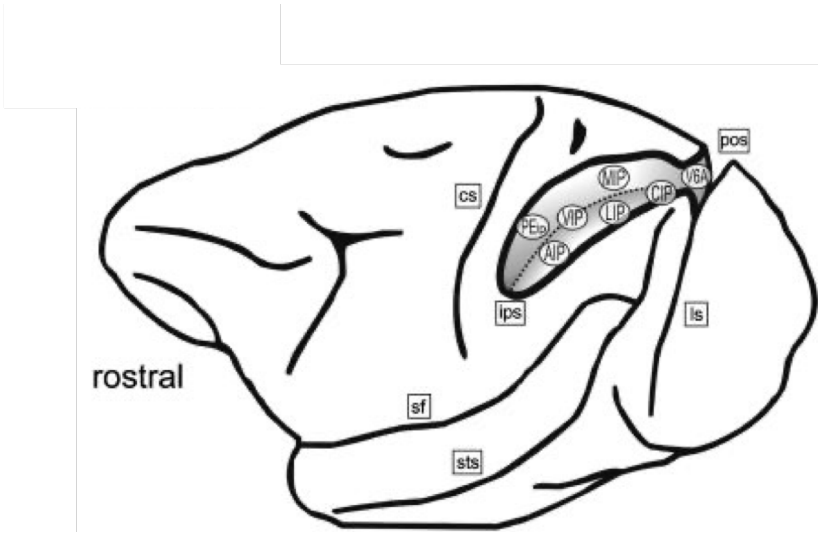

Figure 3. Lateral view of the macaque intraparietal sulcus. The macaque intraparietal sulcus (IPS) is divided into medial (MIP), lateral (LIP), and ventral (VIP) banks. Adapted from Grefkes & Fink, 2005. *Journal of Anatomy. 10.1111/j.1469-7580.2005.00426.x*

The LIP is strongly connected with visual areas, including the FEF and superior colliculus, and is commonly associated with goal-directed saccades. Not only do neurons in this area discharge strongly in response to the detection of salient visual stimuli, but also during the delay period where the animal must recruit their visuospatial working memory to maintain a representation of the target. LIP neurons also discharge when the macaque is cued to make a saccade towards a remembered target location (Grefkes & Fink, 2005). Finally, electrophysiology studies have observed increases in high-frequency activity during memory-delayed saccade tasks, suggesting that the LIP is associated with the coordination of visuospatial attention towards salient objects in space (Bisley & Goldberg, 2003; Pesaran et al., 2002).

The macaque VIP is a polymodal area, and connects and integrates various sensory stimuli, such as tactile, visual, proprioceptive, and auditory signals. In terms of visual stimuli, VIP neurons appear to respond most prominently to visual information in

motion, and represent this information in a predominantly egocentric frame of reference (Grefkes & Fink, 2005). Neurons along the VIP also respond particularly strongly to visual information coming towards the animal's peri personal space (Grefkes & Fink, 2005). Cook and colleagues (2003) microstimulated neurons along the VIP, and observed a constellation of defensive facial expressions made by the monkey, including grimacing, eye closure, and shoulder elevation. Thus, the VIP seems to be most commonly associated with the multisensory orientation of attention, specifically directed towards the monkey's face in a potentially defensive manner. Therefore, the macaque area VIP, along with integrating various sensory signals is also likely associated with defensive physical behaviours.

The monkey PRR area is strongly associated with reaches and saccades to targets, principally encoding spatial location in an egocentric reference frame. Specifically, the IPS is a key multisensory region in both monkeys and humans, and is associated with the integration of visual, somatosensory, proprioceptive, and motor signals to support spatial representations for visually-guided behaviours (Grefkes & Fink, 2005). The IPS is associated with attentional control of eye and limb movements towards salient targets in space, and has thus been very well characterized as an important hub in the domain of visuospatial processing (Grefkes & Fink, 2005; Caspers et al., 2012).

The IPS, most specifically, the LIP, is heavily connected with areas in the frontal cortex, including the FEF and SEF. The FEF receives dense anatomical connections from the LIP and VIP (Blatt et al. 1990; Huerta et al. 1987; Stanton et al. 1995), and although it receives stronger parietal inputs than the SEF, prior studies have established that the SEF nevertheless receives IPS input as well (Huerta & Kaas 1990). Furthermore, more

recent work has clarified the connections between MIP and FEF, and has reported that the MIP receives input from the FEF, F2, and F4/5 (Bakola et al., 2017). Additionally, Ahmed and colleagues (2025) determined that cells on the dorsal and ventral sides of the LIP have distinct profiles, such that dorsal LIP neurons only receive feedforward FEF input, while ventral LIP neurons both provide and receive connections from FEF.

1.4 Local Field Potentials Recorded from Macaques

Local field potentials (LFPs) represent the summed synaptic activity of populations of neurons by aggregating the low-frequency (<500 hertz) extracellular potentials of the cells that are closest in proximity to a depth electrode, allowing for recordings to be taken of the transient activity of local populations of neurons (Einevoll et al., 2013; Maling & McIntyre., 2016). LFPs are classified into five distinct frequency bands: delta (1-4 Hz); theta (4-10 Hz), alpha (8-12 Hz); beta (15-30 Hz); and gamma (30-90 Hz). Previous literature has demonstrated that oscillatory power across frequency bands are important in the context of memory-guided reaching movements in humans and macaques alike (Denker et al., 2018; Esghaei & Reza Daliri, 2014; Heinrichs-Graham et al., 2020; Khayat et al., 2010). For example, in LFP's recorded in the motor, primary motor, and premotor cortices of macaques performing a delayed-to-reach task, Denker and colleagues (2018) observed that beta oscillatory power synchronized during the initialization of the cue to reach, desynchronized during the delay period, and re-synchronized during the arm movement to the target, suggesting that beta oscillatory power, recorded in the motor and premotor cortices could be associated with motor planning and execution.

A common motif recorded from LFP studies in macaques and magneto/electroencephalography studies in humans is referred to as the peri-movement

beta event-related desynchronization (ERD), which occurs 1 second before movement onset, and lasts until 0.5 seconds after the movement has been completed (Heinrichs-Graham, 2020). The peri-movement beta ERD is associated with several cognitive and motor aspects involved in reaching movements, such as movement planning and execution (Kaiser et al., 2001), movement options (Grent-‘t-Jong et al., 2014), and the complexity of the movement (Heinrichs-Graham & Wilson, 2015).

In macaque cortex, visuospatial attention has been consistently associated with the modulation of LFP power (Esghaei & Reza Daliri, 2014; Khayat et al., 2010). Khayat and colleagues (2010) recorded LFPs from macaque area MT, and observed that high-frequency gamma power was modulated by visual motion direction and colour contrast, while <30 Hz frequency bands were modulated by directing attention into a neuron’s receptive field. Esghaei and colleagues (2014) reported that support vector machine decoding of attentional direction was highest in low gamma power, indicating that high-frequency synchrony was associated with directing and coordinating visuospatial attention towards salient targets. Additionally, decoding performance at low frequencies (delta and theta bands) increased as the monkey was attenuating to an anti-preferred direction, suggesting that attention may have more modulating power on lower-frequency bands compared to high-frequency bands.

LFP studies in the IPS during reaching tasks have determined that the IPS is both associated with visuospatial attention and reach planning, suggesting a shared substrate for spatial attention and action-related processing (Mooshagian et al., 2021; Mooshagian & Snyder, 2026; Scherberger et al., 2005). Mooshagian and colleagues (2021) recorded LFPs from the LIP and MIP while a monkey performed either delayed saccades or

reaches to a virtual target, and reported that high-frequency power in the beta band was able to contain information about future arm movements that was unable to be decoded from average spiking output. Additionally, Mooshagian and colleagues (2021) observed an increase in beta power synchrony for contralateral reaches, as well as an initial decrease in power as the target is initially shown, followed by the peri-movement beta ERD associated with the signal-to-reach. Mooshagian and colleagues (2021) hypothesized that these decreases in beta power could reflect the ongoing maintenance of a motor plan.

Scherberger et al. (2005) recorded LFPs while a macaque performed a memory-delayed reaching and saccade task, and observed that during reach planning, mean LFP power (<10 Hz) decreased relative to baseline population activity, while LFP power from 10-100 Hz increased relative to baseline. This increase was also observed during saccade planning (Scherberger et al., 2005). Finally, Chambellant et al. (2024) reported that mean LFP power in the delta-frequency band increased during reaching behaviours, but decreased during grasps (Chambellant et al., 2024).

1.5 Cue Conflict Studies in Humans

Numerous studies in humans have examined the influence of egocentric information (Batista et al., 1999; Blohm & Crawford, 2007; Crawford et al., 2004) and allocentric information (Krigolson & Heath, 2004; Sheth & Shimojo, 2004) on spatial navigation and reaching behaviour. Specifically, Bryne and Crawford (2009) examined how egocentric and allocentric visual information are weighted when both visual reference frames are available by using a maximum-likelihood estimator (MLE) model (Figure 4).

First, human participants completed a memory-guided reach task, where they had to memorize the location of a virtual target relative to a landmark and point to that remembered location under three different conditions: a cue-conflict condition, which involved the landmark undergoing a shift during the memory delay prior to the participant's reach; an egocentric condition, where the participant's reach was not aided by any visual landmarks; and an allocentric-variability condition, where both the landmark and target shifted equally prior to the participant's response. An MLE model was then fitted to this data to extract the allocentric weight that was placed on each condition. During the experiment, an overall average weight of 60% was placed on egocentric information and 40% on allocentric information, indicating that although humans still utilize available allocentric information during reaches, there is more of an emphasis on egocentric information when landmarks are thought to be unstable or unreliable (Byrne & Crawford, 2009).

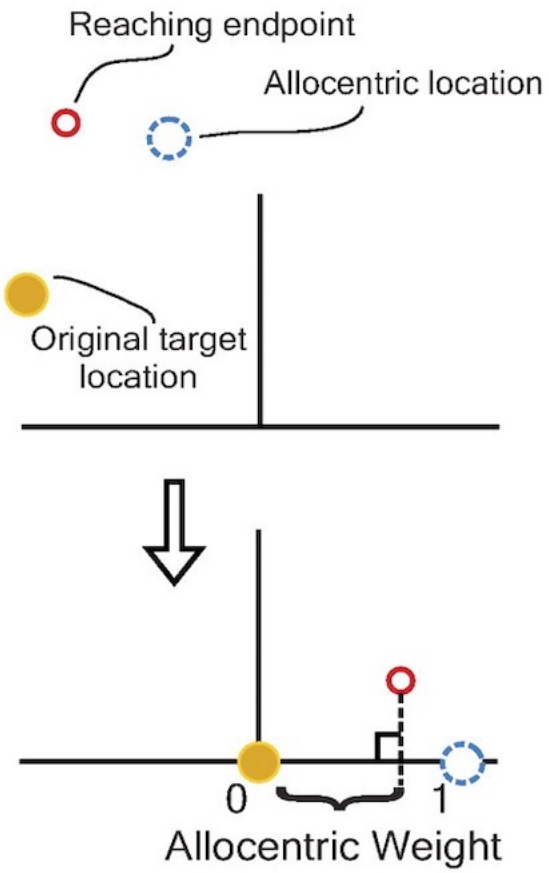

Figure 4. Allocentric weight transformation procedure. Each response (denoted in small red circle) was translated, rotated, and scaled its position vector such that the original target (denoted in solid orange disc) would then be the origin of the new coordinate system. The allocentric location (denoted by large, blue circle) would be at the (1,0) location. Adapted from Byrne, Crawford, 2009. *Journal of Physiology. https://doi.org/10.1152/jn.01008.2009*

Later work has continued to investigate the effect of allocentric and egocentric weighting on cue-conflict studies. For example, Schütz and colleagues (2013) reported that reach endpoint was influenced by a prior gaze shift despite the initial location of the target being foveated. Additionally, the reaching endpoint was overshot in the opposite direction of the gaze shift, indicating that the location of the target may have been remapped onto the gaze periphery. Although reach was modulated by gaze, reach error

varied significantly less when participants were assisted in their reach with a landmark (Schütz et al., 2013).

Fieler et al. (2014) exposed human participants to naturalistic images of a dining room table populated with six common, local objects (coffee mug, plate, butter dish, etc.), along with three common, global objects (table, cloth, painting). Participants freely observed the image until all objects were committed to memory, before observing a brief flash of the same image with one local object missing, and the rest of the objects having undergone some degree of visual distortion. Fiehler and colleagues (2014) observed that mean reaching error increased as the number of local objects in the environment were visually distorted, with errors being most pronounced when the maximum number of local objects were shifted. Additionally, they reported that allocentric weights were highest during trials where all five objects were shifted, relative to trials where fewer local objects returned distorted, indicating that allocentric reliability increased as the variance between local objects decreased. Lu & Fiehler (2020) then perturbed the participant's ability to notice any landmark shift by inducing a light puff of air in the participant's right eye, eliciting a quick blink from both eyes. In line with Fiehler et al.'s previous work (2014) Lu & Fiehler (2020) observed greater reaching errors as more objects were shifted, and the direction of the reaching errors also always followed the direction of the object shifts (right/right, left/left).

Musa et al. (2024) observed that explicit instruction to attend to a visual landmark modulated allocentric weight during a similar cue-conflict paradigm. Participants were instructed to reach with their arm and touch the location of a remembered target with the assistance of a visual landmark at all times. Reaching performance was modulated by

the presence of an audio cue, which explicitly instructed participants to reach relative to the landmark, as opposed to using purely egocentric coordinates to guide the arm reach. When instructed to reach relative to the landmark, participants were faster to perform the reach, along with being more accurate and precise. This effect was further increased when participants reached to the visual field opposite the initial target location (Musa et al., 2020).

1.6 Cue Conflict Studies in Macaques

Macaque electrophysiology and behavioural studies have confirmed the same pattern of results observed in human cue-conflict studies (Bharmauria et al., 2020, 2021; Li et al., 2016; Lin et al., 2024). Li et al. (2016) exposed two macaques to a cue conflict task involving a landmark shift, and observed that the presence of allocentric information pulled the final gaze endpoint in the direction of the landmark. Specifically, when the initial landmark was observed in a closer proximity to the initial eye position, a greater influence on the final gaze endpoint was exerted, suggesting that the primate brain placed more weight on allocentric visual feedback when preparing to move (Li et al., 2016). During landmark shift trials, the weight that the animals placed on allocentric information was 25%, compared to 75% for egocentric information, scaled towards how reliable each reference frame was perceived as being (Figure 5).

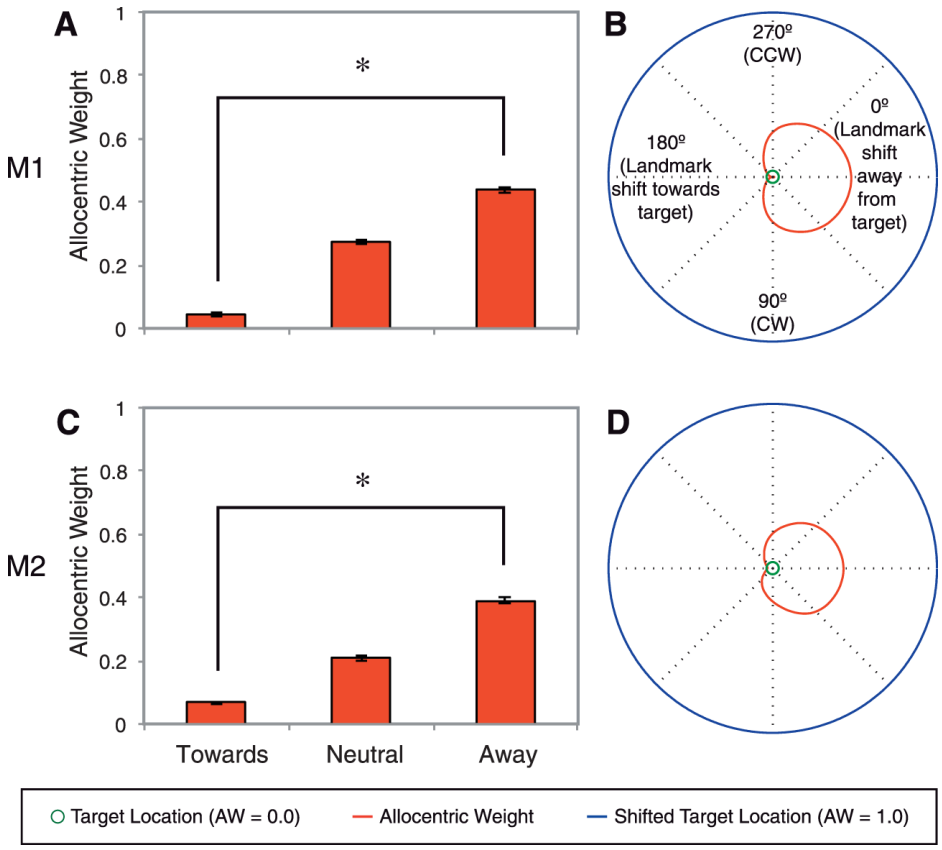

Figure 5. Influence of landmark shift relative to initial target position on allocentric weight. (A) Comparison of the mean AW (Y axis) between landmarks that shift toward or away from the initial target position (X axis) for M1. (B) Overall AW sorted by landmark direction for M1. (C) Comparison of the mean AW (Y axis) between landmarks that shift towards or away from the initial target position (X axis) for M2. (D) Overall AW sorted by landmark direction for M2. Same convention as Figure 7B. Error bars indicate one standard error of the mean; statistical significance is denoted by (*) above the bar graphs. Adapted from Li et al. (2017). *Journal of Vision. https://doi.org/10.1167/17.5.20*

Schütz and colleagues (2023) recorded FEF and SEF activity from two monkeys trained on a saccade task to investigate the influence of landmarks on the visual responses of neurons in these areas, and observed saccades to target, landmark, and target-landmark interactions in the FEF and SEF visual responses. Importantly, this study showed that landmark information remains stable across both areas, and influences the response properties of frontal neurons to stabilize motor responses in the presence of potentially unreliable egocentric information. Further, Bharmauria and colleagues (2020,

2021) recorded primate FEF activity during a cue-conflict memory-guided saccade task where, during random trials, the visual landmark shifted during the memory delay period. After fitting a neural circuit model to their macaque data, Bharmauria et al. (2020) observed that, while visual landmarks were available, FEF visual and motor responses were dominated by egocentric coordinates. However, within the motor code was a shift towards an allocentric coordinate system, first as an unintegrated shift (in other words, uncorrelated with the target-to-gaze transformation), before turning into an integrated shift (or, correlated with target-to-gaze transformation). Bharmauria et al.'s (2020) initial study indicated that the FEF plays a strong role in integrating allocentric and egocentric gaze information. Bharmauria et al. (2021) then used a model-fitting approach to investigate spatial codes in the SEF while a macaque completed a memory-guided saccade task involving another landmark shift, and observed that SEF neurons not only encoded the target position, but also predicted the future gaze location.

Lin et al. (2024) reported that macaque reaches also deviated in the direction of the landmark shift, with an allocentric weight of 29% for arm reaches and 38% for gaze shifts, suggesting that monkeys display the same reaching and gazing behaviour as humans under similar cue-conflict conditions. Lin and colleagues (2024) conducted a memory-guided reach task, where a macaque observed a virtual target briefly flash in front of them on a touch screen, and, following a memory delay, was cued to reach to the remembered target location. During landmark trials, the animal followed the same procedure, but with either a stable landmark visible, which assisted the accuracy of the reach by acting as a reliable allocentric cue; or a shifted landmark, which, following a

mask, shifted by 8° in one of 8 directions, and acted as an unreliable allocentric cue (Figure 6). For this current study, the same memory-guided reach task was used.

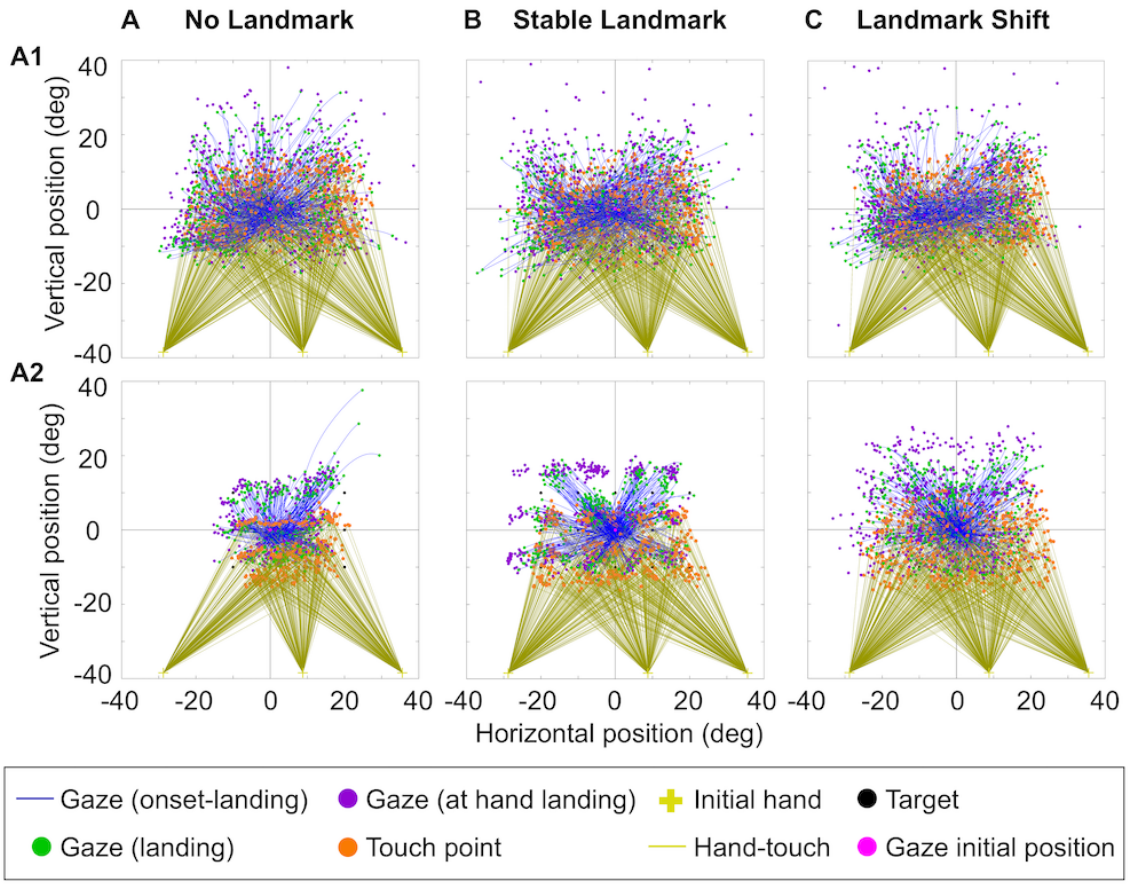

Figure 6. Gaze, head and touch endpoints, and 2-D gaze trajectories for both animals. (A1: monkey L; A2: monkey V). Trajectories are plotted from the time of initial gaze motion to the final hand touch. Complete gaze trajectories are provided, whereas the hand trajectories are only shown as vectors joining the initial and final hand positions.

1.7 Specific Questions and Hypotheses

The behavioural influence of egocentric and allocentric cues has been well characterized in the human and macaque reach system. However, the influence of landmarks and landmark shifts during a memory-guided reaching task on the neural activity within the macaque IPS has not been characterized. For that reason, this current

study examined how allocentric visual information modulates the macaque IPS LFP signal during reaches toward a target. I exposed two female macaque monkeys (*Macaca Mulatta*) to a memory-guided reach task with three conditions: an egocentric, or no landmark (NL) condition, where the monkey had to remember the target location with no other visual feedback; a stable landmark (SL) condition, where the monkey's reach was assisted by the presence of an unmoving landmark on the screen; and a shifted landmark (ShL) condition, where the landmark was surreptitiously shifted prior to reach. As the monkey was completing this task, LFP signals were recorded from the LIP, MIP, and VIP, to investigate the effect that the landmark and landmark shift had on the local activity of neurons within the IPS.

I hypothesized that 1) LFP power during no landmark control trials will significantly differ from baseline activity at rest, such that I expect to observe increases in spectral activity reflecting the memory response as the animal must maintain the representation of the target, as well as the motor response as the animal conducts a reach towards the remembered location; 2) activity during SL and ShL trials will significantly differ from power during NL trials, such that I expect to observe differences in the memory and motor response periods of the task, as the presence of the landmark both reduces the cognitive load that the animal has to maintain to represent the target location, as well as increases the reach accuracy towards the target (Bharmauria et al., 2024; Lin et al., 2024; Taghizadeh et al. 2024); 3) I hypothesize that LFP power during ShL trials will significantly differ from power during SL trials specifically during the hand-onset and hand-touch periods of the task, as, due to the landmark shift, the animal will have to form a different motor plan that accurately integrates both egocentric and allocentric information; 4) and

finally, I expect to observe band-specific differences in activity across all areas (LIP, MIP, and VIP), reflecting the functional division of the areas along the macaque IPS – specifically, I expect to observe increases in LIP and MIP activity during the hand-onset and hand-touch components of the task relative to VIP activity, as both the LIP and MIP have been strongly associated with saccades and arm reaches in the context of goal- and memory-directed actions (Grefkes & Fink, 2005).

CHAPTER 2 POSTERIOR INTRAPARIETAL SULCUS ACTIVITY DURING A HEAD UNRESTRAINED, MEMORY GUIDED REACH TASK

Brando Sheldrick[1-3], Verónica Nácher [1-3],Jennifer Lin[1,2,4], Hongying Wang[1-3], Ashkan Karimi[1-3], Saihong Sun[1-3], Xiaogang Yan[1-3], J. Douglas Crawford[1-4]

1. Centre for Integrative and Applied Neuroscience, 4700 Keele Street, York University, Toronto, Ontario, Canada, M3J 1P3
2. Centre for Vision Research, 4700 Keele Street, York University, Toronto, Ontario, Canada, M3J 1P3
3. Department of Psychology, York University, 4700 Keele Street, Toronto, Ontario, Canada, M3J 1P3
4. Department of Biology, York University, 4700 Keele Street, Toronto, Ontario, Canada, M3J 1P3

2.0 Abstract

In order to efficiently navigate throughout environments and coordinate our effectors to smoothly interact with objects around us, mammals must integrate visual information through two reference frames. In particular, two important sources of visual information are derived through egocentric, or body-centred reference frames, and allocentric, or world-centred reference frames. Prior work has shown that cells along the ventral visual stream primarily encode visual information in an allocentric perspective, while cells along the dorsal stream primarily encode visual information in an egocentric perspective (Goodale & Haffenden, 1998). However, recent research has suggested that the distinction between cells encoding egocentric and allocentric information may not be so clear (Taghizadeh et al., 2024). The main goal of this current study was to investigate the influence of stable and shifted landmarks on local field potential (LFP) activity recorded in the lateral, medial, and ventral banks of the non-human primate intraparietal sulcus (IPS). We collected LFP data from two female *Macaca Mulatta* monkeys (ML) trained to perform a memory-guided reaching task in the dark. Each trial began with the hand fixated at a variable location on a waist-level LED bar while the animal maintained central fixation. During no landmark (NL) trials, a target briefly flashed at a random location, and after a memory delay, the animal was cued to reach to the remembered location. During stable landmark (SL) trials, a landmark (4 dots spaced 10° apart) encapsulated the target and remained visible for the duration of the task; while shifted landmark (ShL) trials were associated with a surreptitious landmark shift of 8° in one of 8 directions following the memory delay. LFP activity differed between the MIP, LIP, and VIP in both animals during the task, suggesting that each bank of the IPS plays a specified

role in the task. Additionally, LFP spectral activity significantly differed from baseline activity during the task, indicating that the task significantly modulated LFP dynamics beyond activity at rest. Finally, Relative to NL trials, LFP data recorded from all IPS sites in both animals was significantly modulated during SL and ShL trials relative to NL trials, but not during SL trials relative to ShL trials.

2.1 Introduction

Mammals are privy to a vast amount of visual information that is effortlessly coordinated with the motor system to allow for a great degree of flexibility and precision when interacting with targets in the environment. Broadly, mammals encode visual information through two specific reference frames. An egocentric, or body-centred reference frame encodes visual information in a coordinate system relative to the location of one's own body in space; while an allocentric, or world-centered reference frame encodes visual information in a coordinate system relative to the location of other objects, or landmarks, in the environment (Moraresku & Vlcek, 2020; Simons & Wang, 1998). These distinctions have been studied extensively in some fields of neuroscience, such as memory and navigation, but much less is known about how egocentric and allocentric information is used and integrated for control of action.

The functional distinction between egocentric and allocentric reference frames has been supported by the long-standing *two-stream hypothesis of vision*, which suggests that the mammalian visual system is divided along a dorsal stream, which projects from the striate cortex to the posterior parietal region (PRR), and a ventral stream; which projects from the striate cortex to the inferotemporal (IT) cortex (Ungerleider & Mishkin, 1982; Goodale & Milner, 1992). The dorsal, or *"where"* stream is predominantly

associated with encoding the physical locations of objects in space, and encompasses regions that support the dynamic and effortless coordination, integration, and transformation of sensory information into the appropriate motor vectors for object interaction. In contrast, the ventral, or *"what"* stream is predominantly responsible for encoding the stable visual and contextual qualities of an object, such as size, colour, texture, and semantic features, for the formation of persistent long-term representations. Due to this specification, cells along the dorsal stream encode moment-to-moment information in an egocentric reference frame, while cells along the ventral stream encode visual information in an allocentric reference frame (Goodale & Haffenden, 1998).

Despite the extensive body of literature characterizing the two streams of vision, it is still largely unclear as to how these two reference frames interact with each other to coordinate the mammalian visual and motor system in such a dynamic and effortless way to support smooth reaching and interacting with objects in the environment. Cue-conflict studies have reported that humans can effortlessly integrate different frames of reference, depending on the situation and the perceived reliability of each reference frame (Bryne & Crawford, 2009). For example, Bryne and Crawford (2009) reported that during a cue-conflict task, where participants were instructed to reach toward a remembered location in the presence of an unreliable landmark, they allocated 20% more weight towards egocentric, rather than allocentric visual information, despite the latter still being readily available in the task. Later cue-conflict studies in macaques have reported that in the presence of an unreliable landmark, macaques similarly shift their relative weight towards an egocentric, rather than an allocentric bias (75% vs. 25%, respectively).

Furthermore, macaque electrophysiological data recorded from the frontal and supplementary eye fields (FEF; SEF, respectively) during a similar memory-guided saccade task reported that the motor and visual activity within these areas updated towards the shifted landmark even when the target itself never moved, indicating that allocentric spatial information is reflected in the motor codes of frontal neurons (Bharmauria et al., 2020; 2021; Schütz et al., 2023). However, these questions have not been studied in the reach system, or in neurons within parietal visual areas such as the lateral (LIP), medial (MIP), and ventral (VIP) banks of the intraparietal cortex.

This current study sought to investigate the influence of stable and shifted landmarks on LFP activity recorded from the LIP, MIP, and VIP from two female rhesus macaque monkeys (*Macaca Mulatta*) during a memory-guided reach task. We hypothesized that 1) LFP power during no landmark control trials will significantly differ from baseline activity at rest, such that we expect to observe increases in spectral activity reflecting the memory response as the animal must maintain the representation of the target, as well as the motor response as the animal conducts a reach towards the remembered location; 2) activity during SL and ShL trials will significantly differ from power during NL trials, such that we expect to observe differences in the memory and motor response periods of the task, as the presence of the landmark both reduces the cognitive load that the animal has to maintain to represent the target location, as well as increases the reach accuracy towards the target (Bharmauria et al., 2024; Lin et al., 2024; Taghizadeh et al. 2024); 3) we hypothesize that LFP power during ShL trials will significantly differ from power during SL trials specifically during the hand-onset and hand-touch periods of the task, as, due the landmark shift, the animal will have to form a

different motor plan that accurately integrates both egocentric and allocentric information; 4) and finally, we expect to observe band-specific differences in activity across all areas (LIP, MIP, and VIP), reflecting the functional division of the areas along the macaque IPS – specifically, we expect to observe increases in LIP and MIP activity during the hand-onset and hand-touch components of the task relative to VIP activity, as both the LIP and MIP have been strongly associated with saccades and arm reaches in the context of goal- and memory-directed actions (Grefkes & Fink, 2005).

2.2 Methods

2.2a Animals and Surgical Procedures

Data were collected from two female rhesus macaque monkeys (*Macaca Mulatta*), monkey V and monkey L. Monkey V weighed 6.5 kg, and monkey L weighed 7 kg during the experiment, and underwent several surgeries, some described previously (Arora et al., 2019). Both animals underwent the exact same surgical procedures. Under general anesthesia (intramuscular injection of 10 mg/kg ketamine hydrochloride, 0.05 mg/kg atropine sulphate, and 0.5 mg/kg acepromazine, followed by 1.5% isoflurane), a steel head post was implanted onto the animal's skull using an acrylic head cap. A Teflon-coated search coil was implanted in both eyes subconjunctivally, along with a scleral coil being placed in the eye to capture horizontal and vertical eye rotation. Both animals recovered for two weeks prior to commencing the experiment. During the data collection period, fluid intake was controlled as both animals were rewarded with water during correct trials. All surgical and experimental protocols followed the Canadian Council for

Animal Care guidelines, and the use of laboratory animals was reviewed and approved by the York University animal care committee.

2.2b Experimental Setup

The experimental setup was described in Lin et al. (2024). The animals were seated in a customized Crist primate chair, and wore a head restraint, top plates to prevent the animal from climbing out of the chair, a security vest, a shoulder collar, and an upper-arm Velcro sleeve that prevented the animal from using their left arm. A chain was fastened from their security vest to the back of the chair, securing the animals comfortably from within the chair. Both animals learned to place their hand on an LED touch bar situated to the chair comfortably at waist level, with the centre of the bar 16cm ahead and 28cm below the right shoulder. The three LEDs on the bar were located (-19°, -64°), (19°, -64°), and (45°, -64°) in the horizontal and vertical axes. Infrared light monitored the position of the monkey's hand, and a sensor above the LED bar detected whether the LED light was blocked by the animal's hand. Both animals observed a touch screen 27 cm away from their eye, which was surrounded by a frame which measured their hand contact with the screen using vertical and horizontal infrared sensors. The task was projected onto the touch screen using a laser projector (Figure 7).

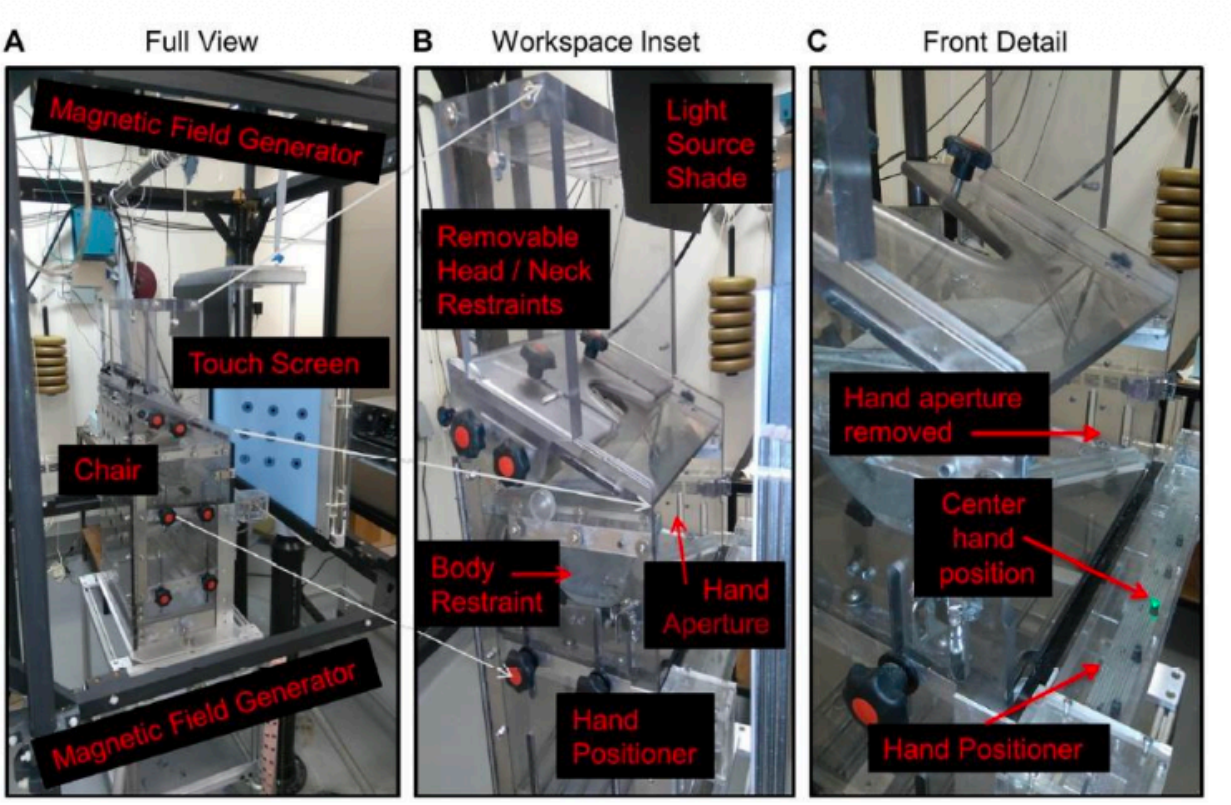

Figure 7. Laboratory setup. (A) A touch screen will be placed in front of the Crist primate chair. (B) The head/neck restraints will be removed during the duration of the experiment, to accommodate naturalistic head movements. The body restraint was a vest attached to the inside of the chair, which comfortably secures the monkey's body. (C) The cue to direct the monkey's hand position was composed of an LED touch bar attached at waist level to the chair at a comfortable distance away from the animal's right hand. Depending on which LED light illuminates prior to the beginning of each trial dictates where the animal places their hand. Adapted from "Eye-head-hand coordination during visually guided reaches in head-unrestrained macaques", by Arora, H. K., Bharmauria, V., Yan, X., Sun, S., Wang, H., & Crawford, J. D., 2020, *Journal of Neurophysiology, 122(5), 1946–1961. Copyright 2019 by the American Physiological Society.*

A steel head post stabilized the monkey's head while the experimental setup was prepared. The 2D eye coil, reward tube, and fluid dispenser were attached to the animal's head cap, along with two orthogonal search coils, which recorded the animal's 3-D head rotations in space. We conducted two separate calibrations before beginning the task. First, the animal was required to fixate on nine targets displayed on screen for 1s, and

second, the 2D magnetic field was precalibrated by rotating an external coil through each direction and adjusting the field strength to an equal maximum.

2.2c Experimental Paradigm

The experiment was conducted in total darkness to eliminate all other stimuli from affecting the animal's performance. All visual stimuli were presented in red, with the target being displayed in the highest intensity. Depending on the trial, the animal observed either an egocentric cue, which was a fixation dot in the centre of the screen which the animal remained fixated on for the duration of the trial until cued otherwise; and an allocentric landmark, which was four identical dots surrounding the target positioned at the vertices of a square with a 10° edge length. The landmark was located at 15 possible randomized locations within a 50° by 30° rectangle located at the bottom-left quadrant of the touch screen. The target was located at one of 14 possible locations within a 5° diameter circle within the centre of each landmark (Figure 8A). The landmark was randomly shifted by 8° in eight possible directions (up, down, left, right, and diagonally) during landmark shift trials (Figure 8A). "Catch trials" were randomly interspersed throughout the task, and involved the target flashing outside the bounds of the landmark rather than within the landmark to ensure that the animal was actually reaching towards the target (Figure 8B).

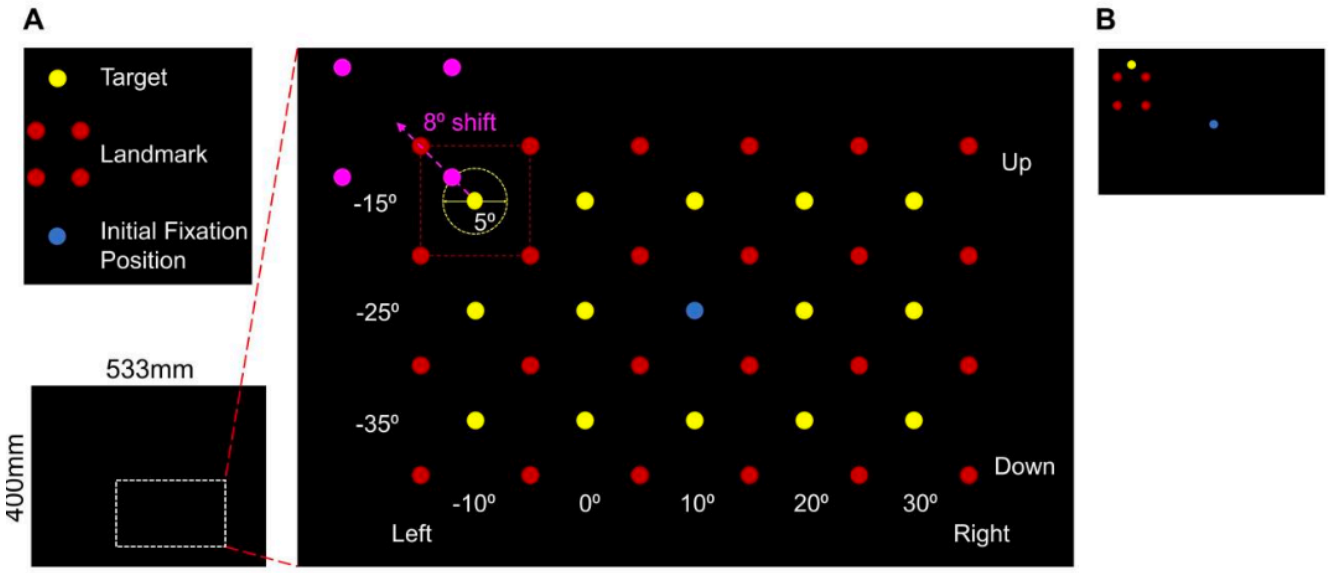

Figure 8. (A) All the possible locations of the target (in yellow) and the landmark (in red). All of the possible corresponding target and landmark locations are displayed here, with the target always appearing within a 5° diameter circle within each landmark. The pink landmark displays the landmark shift by 8° during shifted landmark trials. (B) A "catch trial", where, instead of the target appearing within the landmark it flashes outside the boundary of the square, ensuring the animal is actually attempting to point to the target and not to the middle of the landmark. Adapted from "Influence of a visual landmark shift on memory-guided reaching in monkeys" by Lin, J., Wang, H., Sun, S., Yan, X., & Crawford, J. D., 2024, *Journal of Neurophysiology, 122(5), 1946–1961. Copyright 2024 by the American Physiological Society.*

The experiment was composed of 3 conditions: 1) no landmark; 2) stable landmark; and 3) a cue-conflict condition with a shifted landmark. Each trial began when the animal fixated their hand on the illuminated bulb on the LED touch bar for a period of 700 ms. The fixation dot appeared for 300 ms, which the animal remained fixated on until cued to saccade freely. In conditions 2 (SL) and 3 (ShL), both the fixation dot and the landmark appeared on screen for 500 ms. Failure to acquire or maintain these hand and gaze fixation positions until the final 'go' signals resulted in an aborted trial with no reward. The monkey observed the target flash in their periphery for 100 ms, which preceded a 300 ms delay where the animal only observed the central fixation dot and/or the landmark.

A bright red mask occluded the screen for 200 ms, which concealed any obvious motion of the landmark that would occur during ShL trials, along with preventing any aftereffects caused by the illumination of the target and landmark, forcing the animal to rely solely on their memory instead of any possible target afterimage. Following the mask, the landmark reappeared, either in the same location during SL trials, or shifted by 8° visual angle in one of eight directions during ShL trials. The monkey then had a period of 2000 ms to reach with their right hand and touch the screen in the remembered target location. The animal received a reward of water when they touched the screen within a 5.2 cm radius circle of the target (Figure 9).

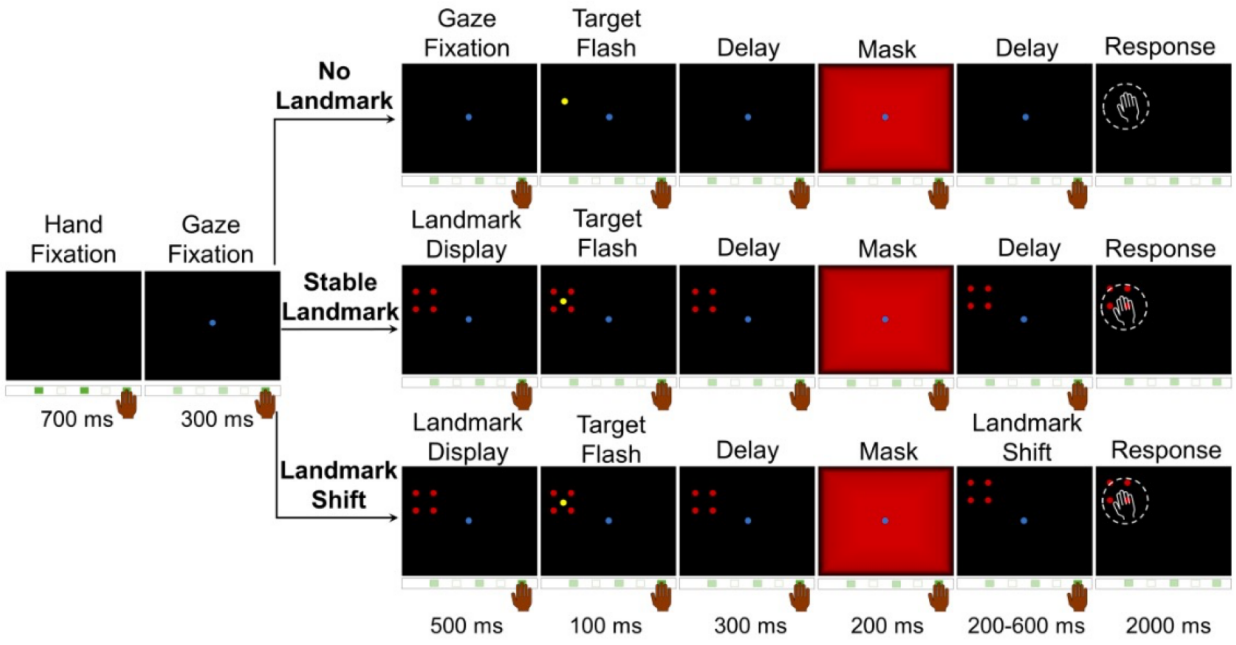

Figure 9. Experimental task and timing. This figure displays the visual information the animal observes throughout the time-course of the experiment. The blue dot is the fixation cue, which the animal remains fixated on throughout the duration of the experiment. The yellow dot is the target, and the four red dots display the visual landmark.

2.2d Data Acquisition

Here, we report data from 18 recording sessions from monkey V and 11 recording sessions for monkey L, with up to 467 trials per session. Animals were implanted with 2D and 3D scleral search coils in their left eyes to monitor eye movements (Robinson et al., 1963; Crawford et al., 1999; Klier et al., 2003). These eye coils enabled us to track both 2D and 3D eye movements (gaze) as well as the orientation of the eyes (including horizontal, vertical, and torsional components relative to space). Additionally, two head coils that were oriented orthogonally to each other were mounted in each recording session to capture head orientation in space. The data obtained from the 2D and 3D eye and head coils facilitated the computation of various other parameters, such as the orientation of the eye relative to the head, as well as eye-velocity, head-velocity, and their respective accelerations (Crawford et al., 1999).

Animals were implanted with a recording chamber centred in stereotaxic coordinates at 6 mm posterior and 7 mm lateral (Paxinos et al., 2009) (Figure 10). A craniotomy of 19 mm (diameter) that covered the chamber base (adhered over the trephination with dental acrylic) allowed access to the left intraparietal sulcus areas (MIP, LIP and VIP). Unfortunately, the probe that was used for monkey L's recordings was too short to record from the VIP, and a longer probe would bend if used. To fix this problem in monkey V, we cut the length of the chamber down, so we would be able to access the VIP without using a longer probe and risking it bending during the recording. Extracellular single-unit activity and LFPs were recorded with a Plexon V-form Probe (32 contacts, 75 um spaced). Recordings were conducted in the left hemispheres of the two monkeys, contralateral to the responding arm. In a typical daily recording session, the initial search

for neurons occurred while the animal's head was fixed. The objective was to find neurons that exhibited clear and consistent spiking activity. Once such neurons were identified, the head of the animal was released, and the experiment started.

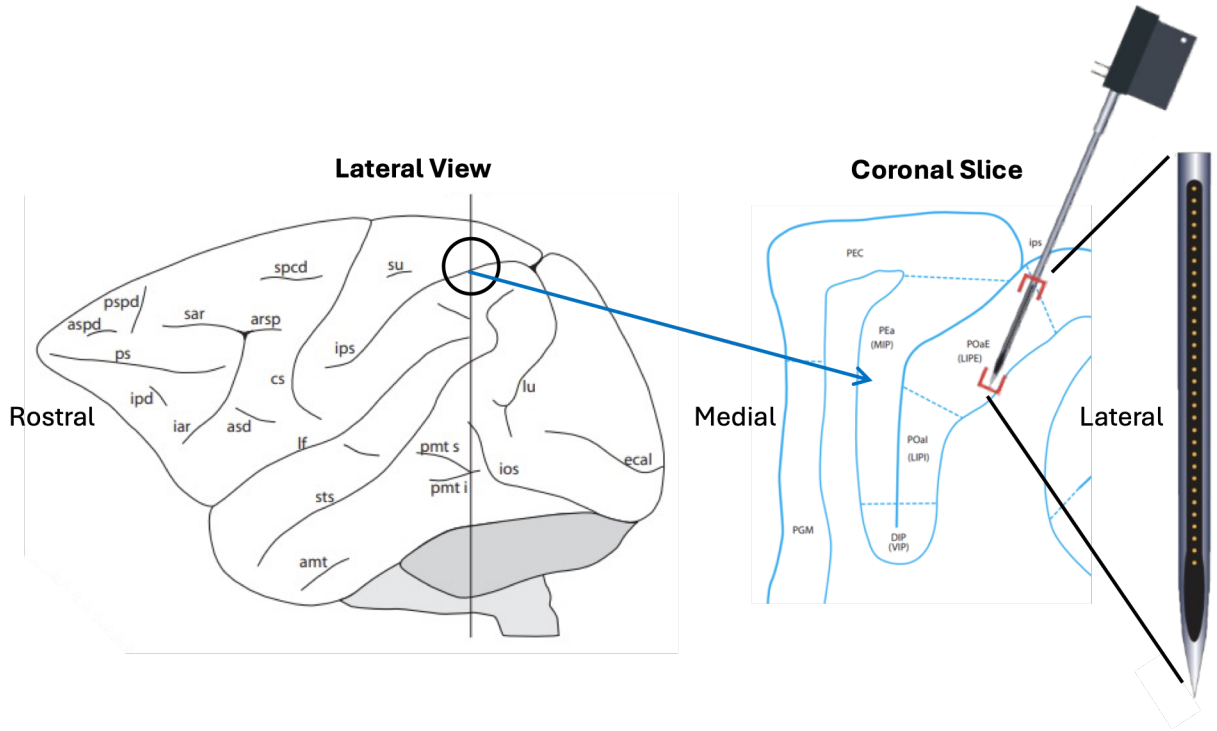

Figure 10. Chamber coordinates. Coordinates of the chamber over both animal's left hemisphere IPS, allowing for acute recordings to be conducted in the LIP, MIP, and VIP using a stainless steel 32-channel Plexon V-form Probe, visualized to the right of the coronal slice of the macaque brain (stereotaxic coordinates anterior 2.1, lateral 40.2). The enlarged portion of the probe displays the 32 channels.

2.2e Data Analysis

LFP data were preprocessed using a custom-built, automated Matlab code to clean the data and remove incorrect or "messy" trials. The code calculated the median values of four metrics for each LFP signal recorded during every trial across all 32 channels: jump; amplitude; drift; and variance. If any trial were to deviate by 3.29 standard deviations above or below the median for three out of the four metrics, the trial was excluded. This preprocessing step was crucial to ensure that we properly removed

artifacts due to head motion and electrical or magnetic interference from our dataset (Leys et al., 2013). For data analysis we used a custom-build Matlab code and the FieldTrip toolbox (www.ru.nl/neuroimaging/fieldtrip). The data were down-sampled offline to a sampling frequency of 1 kHz. Only correct trials (i.e., trials that were rewarded) were included in the analysis. LFPs were analyzed from sessions recording in the MIP (4 sessions for monkey V; 9 sessions for monkey L), the LIP (4 sessions for monkey V; 2 sessions for monkey L), and the VIP (4 sessions for monkey V), with a maximum of 1130 trials per session.

2.2g Spectral Analysis

Time–frequency representations of LFP activity were computed using the FieldTrip toolbox in MATLAB using Hann-tapered Fourier decomposition. Spectral power was averaged across recording channels before statistical analysis. Within-trial comparisons between activation and baseline epochs were performed using a cluster-based permutation paired t-test. Between-condition comparisons were performed using a cluster-based permutation independent-samples t-test. Statistical testing was restricted to frequencies between 4–36 Hz. For both analyses, adjacent significant time–frequency bins ($p<0.05$, uncorrected) were grouped into clusters, and cluster significance was assessed using the maximum cluster-sum statistic with 1000 Monte Carlo permutations. Multiple comparisons across time–frequency bins were controlled using nonparametric cluster-based permutation correction implemented in FieldTrip. Adjacent significant bins ($p<0.05$, uncorrected) were grouped into time–frequency clusters, and cluster significance was assessed using the maximum cluster-sum statistic across 1000 Monte Carlo permutations. This procedure controls the family-wise error rate across the entire

time–frequency space. All tests were two-sided with cluster-corrected significance threshold of $p<0.05$. Both delta and gamma bands were excluded from analysis. First, we were unable to reliably estimate delta-band power, as the relatively short analysis window did not contain sufficient low-frequency cycles to produce stable spectral estimates. Secondly, we restricted our analysis to lower-frequency bands (< gamma), as these exhibited more stable LFP signals across sessions, whereas gamma-band activity is known to be more susceptible to noise and non-neural contamination (Hipp & Siegel, 2013).

2.2h Statistical Analysis

A series of two-way analyses of variance (ANOVAs) were conducted to examine delta-, theta-, alpha-, and beta-band activity across task conditions. Separate ANOVAs were performed for each time window (target flash, hand onset, and hand touch). For each analysis, area (e.g., LIP, MIP, and VIP) and condition (NL, SL, and ShL) were included as within-subject factors. Delta band activity was included in this analysis due to the use of averaged LFP power estimates across sufficiently long temporal windows for low-frequency spectral estimation.

2.4 Results

These data reported here were recorded using in the same task and one animal (monkey L) reported in Lin et al. (2024), which showed: 1) a typical temporal sequence of gaze followed by reach movements toward targets; 2) relatively inaccurate gaze shifts (compared to reach) following the delay period; 3) a significant improvement in reach precision in the presence of a stable landmark, and; 4) reach allocentric weight of .29 (animal L) in the landmark shift condition. Here we report the neural events that accompany this behaviour, focusing on the timing of events relative to target presentation, reach onset and final touch.

2.4a Oscillatory Dynamics during the Memory-Guided Reach Task

Throughout all conditions of the task, both animals displayed LFP spectral activity that was modulated by the specific task demands associated with NL, SL, and ShL trials. To illustrate an example of such spectral modulations, Figure 11 displays the LFP activity recorded in monkey V's LIP, MIP, and VIP (rows) during NL, SL, and ShL trials (columns), with the data temporarily aligned to the home fixation period. To briefly summarize the activity that was recorded in these areas, spectral activity in the MIP was characterized by early, low-frequency desynchronization during NL trials, which increased into low-frequency synchronization towards the end of the trial. Additionally, there was a decrease in activity in the higher-frequency bands during the same period (Figure 11A). This pattern of activity increased during SL (Figure 11B) and ShL (Figure 11C) trials, such that desynchronized activity in the lower- and higher- frequency bands was more pronounced, especially towards the end of the trial. Activity in the MIP across NL (Figure 11D), SL

(Figure 11E), and ShL (Figure 11F) trials was characterized by substantial desynchronization in the low- and high-frequency bands, with spectral activity reaching a nadir at approximately 2 seconds post-home fixation in all conditions. Similar to LIP activity, the pattern of desynchronization in the MIP seemed to increase during SL trials. Finally, activity in the VIP displayed later, low-frequency desynchronization following the mask period during NL trials (Figure 11G). During SL (Figure 11H) and ShL (Figure 11I) trials, there was a substantial increase in desynchronization during the target flash periods, as well as during the later periods towards the end of the trial in monkey V's VIP.

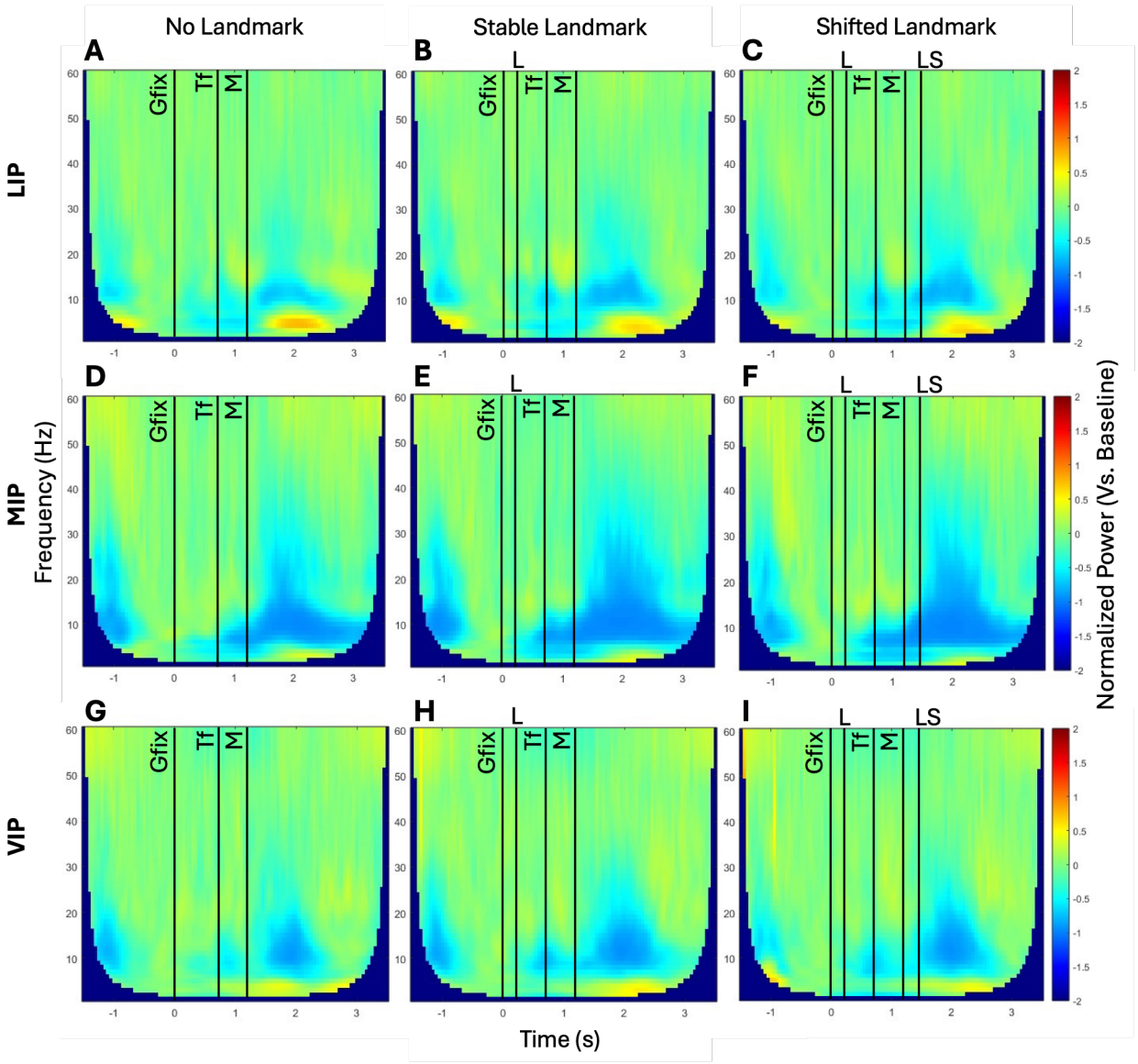

Figure 11. LFP oscillatory dynamics during the reaching task. (A, B, C) LFP spectrograms aligned to the home fixation event for monkey V, averaged across all recording dates in the LIP and divided across no landmark (NL) (A), stable landmark (SL) (B), and shifted landmark (ShL) (C) trials. (D, E, F) LFP spectrograms aligned to the home fixation event for monkey V, averaged across all recording dates in the MIP and divided across NL (D), SL (E), and ShL (F) trials. (G, H, I) LFP spectrograms aligned to the home fixation event for monkey V, averaged across all recording dates in the VIP and divided across NL (G), SL (H), and ShL (I) trials. The vertical lines illustrate the average time of different events: gaze fixation (Gfix, 0 s), landmark on (L, 0.3 s), target flash (Tf, 0.8s), mask on (M, 1.2 s), and landmark shift (LS, 1.4 s).

2.4b Frequency-Dependent Oscillatory Power in the Memory-Guided Task

We first investigated the differences in LFP oscillatory power across our three recording sites during NL trials of the task relative to power at baseline, which we defined as a 500 ms window of time during the home fixation period that preceded every trial. Figure 12 shows average data across experiments that were significantly different from baseline for monkey V (top three rows) and L (bottom two rows), aligned on target onset (A), hand movement onset (B) and final hand touch (C).

LFPs recorded in the MIP in monkey V displayed patterns of oscillatory power that significantly differed from LFP power at rest (Figure 12A, B, C). During the target flash event, activity in monkey V's MIP displayed significant high-frequency activity that tapered off 2 ms after the flash. There was additional activation in the high-alpha band that persisted until the end of the event, along with significant desynchronization in the theta and alpha bands that also persisted until the end of the target flash period. Activity in monkey V's MIP during the hand onset (Figure 12B) and hand touch (Figure 12C) events of the task displayed significant low- and high-frequency desynchronization that persisted for the duration of both events. The only deviation from this pattern occurred 300 ms into both hand onset and hand touch events, where there was a brief, yet significant period of low-frequency synchronization in the theta band that significantly differed from baseline spectral activity (Figure 12E, F).

LFP activity recorded in monkey L's MIP also displayed significantly different patterns of spectral activity relative to baseline during the target flash period, as well as during both hand onset and hand touch events of the task (Figure 12J, K, L). During the target flash period, there was initial significant high-frequency synchronization in the beta-

band, that persisted until approximately 200 ms post-target flash. Additionally, there was significant high-frequency synchronization in the alpha band, that steadily increased into the beta band and persisted for the remainder of the target flash event. Furthermore, there was also high-frequency synchronization in the high-beta band (>25 Hz) that began immediately following the target flash, and continued for approximately 500 ms post-target flash. There was also mild, yet significant desynchronization in the theta band beginning 200 ms after the target flash until the end of the target flash period (Figure 12J). Activity during the hand onset and hand touch events of the task in the MIP was dominated with significant low- and high-frequency synchronization during these two epochs relative to baseline (Figure 12K, L).

We did not obtain any VIP sites from monkey L, but LFPs recorded in monkey V's LIP displayed spectral activity that significantly differed across target flash, hand onset, and hand touch task events relative to baseline LFP activity (Figure 12D, E, F). During the target flash event, activity did not significantly differ from baseline until approximately 200 ms post-target flash, where there was a small, yet significant increase in synchronization in the alpha and beta bands that persisted for approximately 100 ms, before activity once again ceased to significantly differ from activity at rest (Figure 12D). During the hand onset period, activity in the LIP displayed significant low- and high-frequency synchronization relative to baseline (Figure 12E). This pattern similarly persisted into the hand touch event of the task, but began to decrease slightly in intensity 200 ms post-hand touch, before diminishing 400 ms after the hand touch, after which activity did not differ significantly from baseline (Figure 12F).

LFP activity recorded in monkey L's LIP displayed significantly different patterns of spectral activity for the hand onset and hand touch, but not target flash components of the task (Figure 12M, N). Relative to baseline activity, LFP oscillatory power in the LIP during the hand onset period displayed significant low- and high-frequency activity throughout nearly all frequency bands (theta-beta), that was sustained until the end of the hand onset period (Figure 12M). We observed the same pattern of activation during the hand touch component of the task in the LIP, albeit with an even stronger pattern of significant high-frequency activity post-hand touch (Figure 12N).

LFPs recorded in monkey V's VIP significantly differed from baseline activity during target flash (Figure 12G), hand onset (Figure 12H), and hand touch (Figure 12I) events of the task. During the target flash period in the VIP, there was mild, yet significant high-frequency desynchronization in the beta band that extended downwards into the alpha band as the task progressed. During this period, there was also mild synchronization in the theta frequency band that extended upwards into the alpha and beta bands, and towards the end of the target flash period there was high-frequency synchronization in the alpha and beta frequency bands (Figure 12G). During the hand onset task event, LFP activity in the VIP (Figure 12H) was very similar to the oscillatory power recorded in the same animal's MIP (Figure 12E), such that there was significant, high-frequency desynchronization that occurred during the onset of the motor movement until the end of the event. As the task event progressed, activity in the higher-beta band (>25 Hz) began to decrease, however, activity in the lower-beta and alpha bands remained consistently desynchronized for the duration of the hand onset event (Figure 12H). Finally, LFP activity recorded during the hand touch event of the task in monkey V's VIP displayed early

desynchronization in the beta band, which trended downwards into the alpha band as the event progressed. Approximately 300 ms after the hand touch, there was an increase in synchronous activity beginning in the theta band and extending upwards into the higher-frequency bands, which continued to increase as the trial progressed, such that, at the end of the trial, LFP power in the alpha and beta bands was strongly synchronized (Figure 12I).

In summary, we observed a constellation of task-related modulations in activation during NL trials relative to LFP power at rest. The most striking similarities between animals seem to be the clear increase in power across the range of frequency bands during the motor periods of the task (i.e., hand onset and touch) in the LIP relative to baseline. However, the LFP activity recorded in each animal's MIP during the same motor periods displayed an opposite pattern of results, such that spectral activity in monkey V's MIP was highly desynchronized, while monkey L's MIP displayed a strong increase in activity. Finally, the spectral activity during the target flash period was less pronounced in both animals, especially in the LIP. Monkey L displayed no significant differences between baseline activity and LFP activity recorded during the target flash period, while monkey V displayed a very minor, yet significant increase in spectral activity in response to the target appearing.

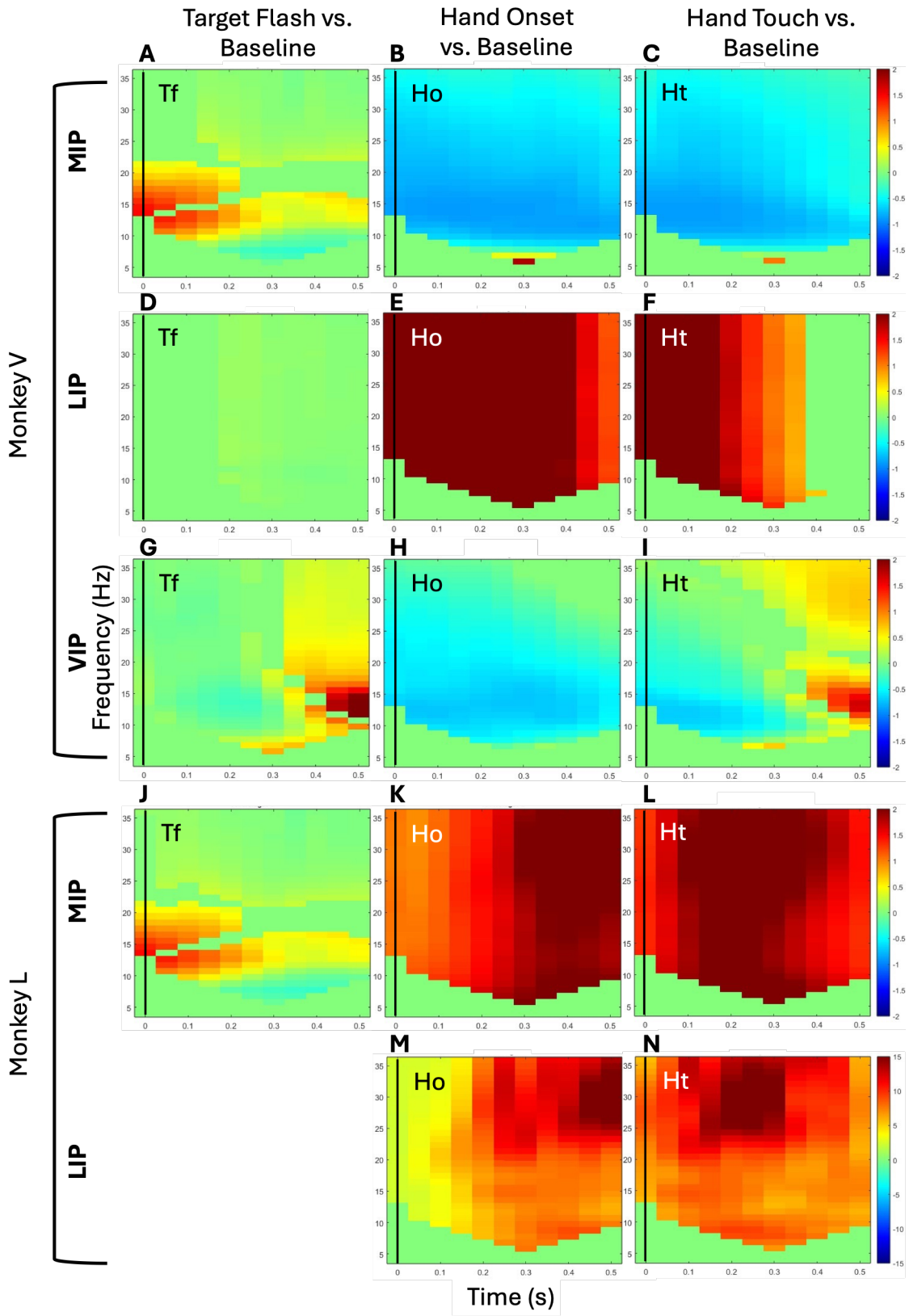

Figure 12. Significant modulations in LFP power relative to baseline across no landmark (NL) trials. (A-I) LFP time-frequency spectrograms averaged across all dates recorded in

monkey V's medial intraparietal sulcus (MIP) (A-C), lateral intraparietal sulcus (LIP) (D-F), and ventral intraparietal sulcus (VIP) (G-I), aligned to the target flash (Tf) (column 1), hand onset (Ho) (column 2), and hand touch (HT) task events (column 3). LFP power spectra displays significant modulations in activity during each task event relative to baseline activity. (J-L) LFP time-frequency spectrograms averaged across all dates recorded in monkey L's MIP (J-L) and LIP (M and N) aligned to Tf (column 1), Ho (column 2), and HT task events (column 3). LFP power spectra displays significant modulations in activity during each task event relative to baseline activity. All task events (Tf, Ho, and Ht) are aligned to time 0.

2.4c Influence of Landmark on LFP Oscillations

Here, we investigated the differences in LFP activity during the same three task events (target flash, hand onset, and hand touch), but now comparing activity during egocentric vs. allocentric trials to examine the impact that the presence of a landmark had on the local activity of neurons along the IPS. To examine this relationship, we separated out trials with NL, trials with a SL, and trials with a ShL. First, we consider the influence of the stable landmark. Figure 13 shows this influence using the same conventions as Figure 12.

LFP activity recorded during SL trials differed significantly from activity recorded during NL trials during all task events in all recorded areas (LIP, MIP, and VIP) in monkey V (Figure 13A-I) and in monkey L (Figure 13J-L). During the target flash event in monkey V's MIP, there was a significant, sustained pattern of desynchronization in the theta and alpha bands that appeared during the target flash and continued for approximately 500 ms (Figure 13A). This period of lower-frequency desynchronization was followed by higher-frequency synchronization in the high-alpha- and beta bands, that peaked around 200 ms after the target flash and gradually decayed over the following 300 ms. During the hand onset period, SL trial activity in the MIP displayed significant high-frequency desynchronization relative to NL trials, which persisted throughout the entire duration of

the hand onset epoch (Figure13B). Additionally, there was significant low-frequency activation in the theta band, which lasted for approximately 300 ms post-hand onset. This pattern was very similar to the significant LFP modulations observed during the hand touch event (Figure 13C). Power in the alpha band remained relatively similar, with a slightly earlier drop-off in significant activation at approximately 270 ms post-hand touch. The strong, significant desynchronization in the beta band continued to dominate this period as well, lasting until the end of the trial.

For SL trials recorded in monkey L's MIP, there were no significant differences in activation relative to NL trials during the target flash period, however, there were significant differences in LFP activation in both the hand onset (Figure 13J) and hand touch (Figure 13K) events. During the hand onset period, there was strong, significant low- and high-frequency activation across the range of frequency bands, that persisted until approximately 400 ms post-hand onset (Figure 13J). For the hand touch period, there was a similar pattern of low- and high-frequency activation, which tapered off approximately 200 ms post-hand touch. However, the same pattern of spectral activity returned 100 ms later, and continued until the end of the trial, save for a small period of approximately 100 ms where activity in the 12-20 Hz range did not significantly differ from NL trials (Figure 13K).

The target flash event recorded in monkey V's LIP during SL trials displayed the least amount of significant power modulations relative to NL trials (Figure 13D). However, there was still a significant increase in high-frequency alpha and beta power that occurred 1 ms after the target flash, and lasted for approximately 2.5 ms. During the hand onset event in the LIP, there was very strong, significant synchronization across the entire range

of frequency bands, which lasted until the end, save for a very brief period of non-significant activity in the high beta- (>30 Hz) band at the very end of the event (Figure 13E). During the hand touch event in monkey V's LIP, there was a similar pattern of significant low- and high-frequency activity that began 100 ms after the hand touch, and persisted until the very end of the trial (Figure 13F). For the NL vs. SL contrast recorded in monkey L's LIP, there were no significant differences in LFP activation during the target flash and hand onset period, but there were significant differences in the hand touch event of the task in SL trials relative to NL trials (Figure 13L). Approximately 200 ms post-hand touch, there was a strong increase in significant high-frequency beta synchronization, which remained until the end of the trial.

LFP power during SL trials relative to NL trials in monkey V's VIP during the target flash event displayed early, lower-frequency synchronization in the theta and alpha bands, along with high-frequency synchronization in the high-alpha and beta bands, which lasted for approximately 300 ms (Figure 13G). Following the decay of the beta desynchrony, synchrony in the alpha and beta band persisted until the conclusion of the target flash epoch. During the hand onset event recorded in the VIP, there was a similar pattern of high-frequency desynchronization (Figure 13H). However, this pattern of desynchronization occurred later in the trial (100 ms after hand onset). There was also an increase of late, low-frequency power in the theta band, which occurred nearly 300 ms after hand onset. Finally, this pattern of activity persisted into the hand touch event, which began with strong, significant beta desynchrony that reversed at the end of the trial into significant, high-frequency synchronous activity (Figure 13I). Furthermore, this event was

also characterized by an increase of significant and sustained low-frequency activation in the theta band.

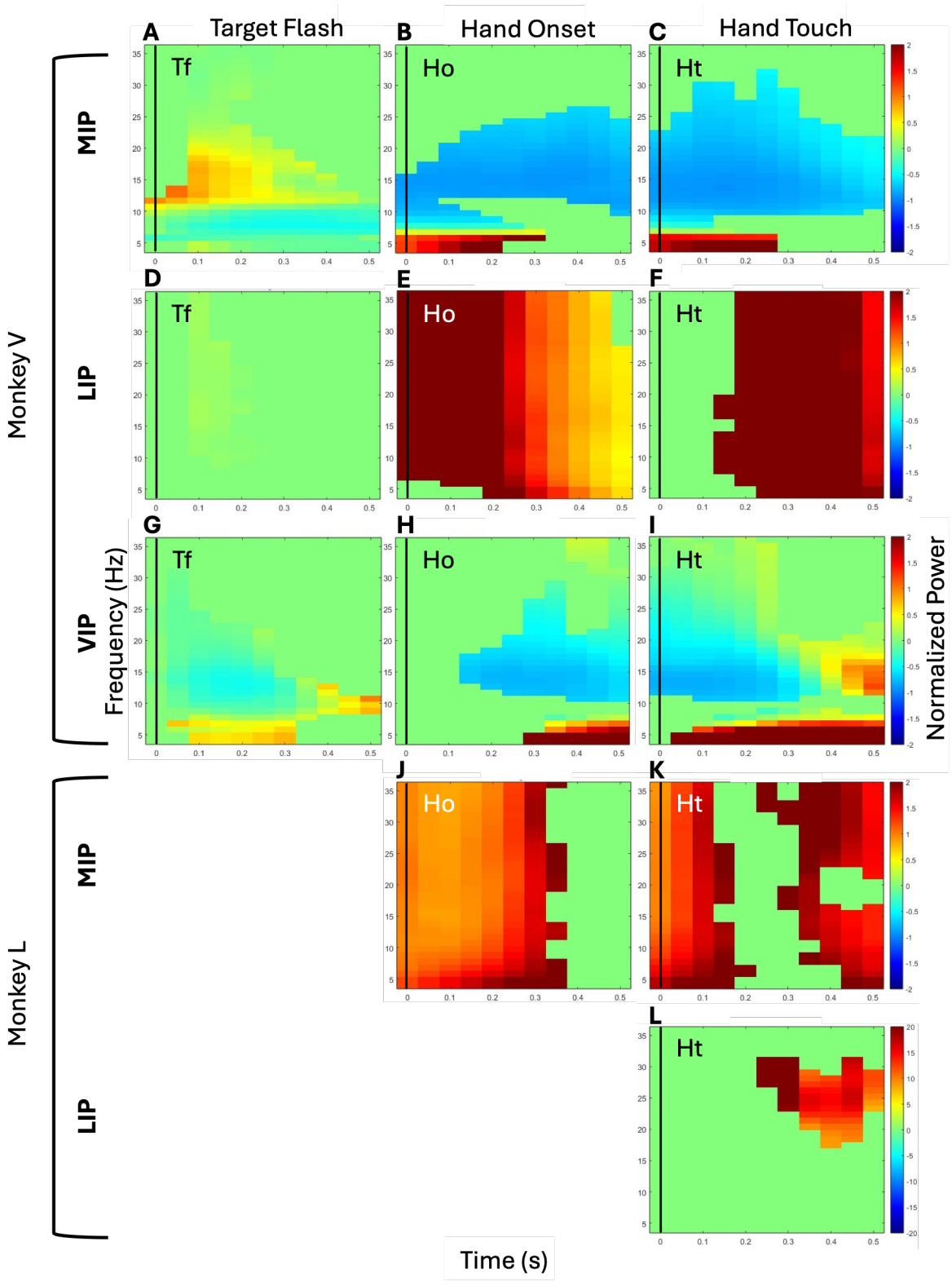

Figure 13. Significant modulations in LFP power during stable landmark trials relative to no landmark trials. (A-I) LFP time-frequency spectrograms averaged across all stable landmark (SL) trials recorded in monkey V's medial intraparietal sulcus (MIP) (A-C),

lateral intraparietal sulcus (LIP) (D-F), and ventral intraparietal sulcus (VIP) (G-I), aligned to the target flash (Tf) (column 1), hand onset (Ho) (column 2), and hand touch (HT) task events (column 3). LFP power spectra displays significant modulations in activity recorded during SL trials during each task event relative to activity during the same events recorded throughout no landmark (NL) trials. (J-L) LFP time-frequency spectrograms averaged across all SL trials recorded in monkey L's MIP (J, K) and LIP (L) aligned to Ho (column 2) and HT task events (column 3). LFP power spectra displays significant modulations in activity recorded during SL trials during each task event relative to activity during the same events recorded throughout NL trials. All task events (Tf, Ho, and Ht) are aligned to time 0.

Figure 14 shows data similar to Figures 12 and 13 except now showing the ShL data relative to NL controls. Spectral activity from both monkeys during ShL trials relative to NL trials displayed nearly the same pattern as activity during the SL vs. NL comparisons, with the only substantial difference occurring during the target flash event in monkey V's LIP, where there were no significant differences in activity between NL vs. ShL trials (Figure 14). Otherwise, significant LFP activation during ShL trials relative to NL trials remained nearly identical to activity during SL trials relative to NL trials. Finally, when we contrasted SL and ShL data we found no significant difference in any area.

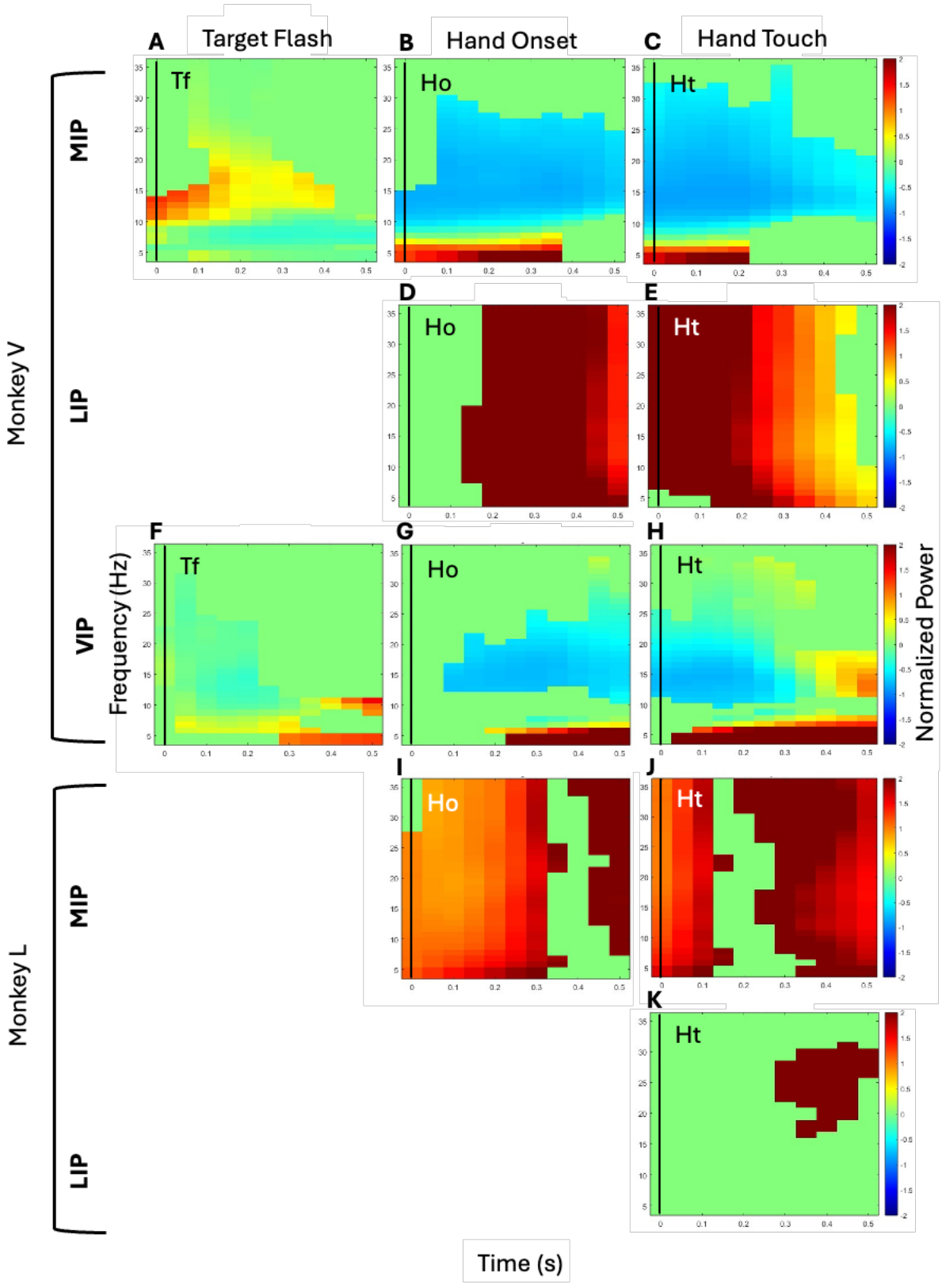
A
Target Flash
B
Hand Onset
C
Hand Touch
Tf
Ho
Ht
D
E
F
G
H
I
J
K
Monkey V
Monkey L
MIP
LIP
VIP
Frequency (Hz)
Normalized Power
Time (s)

Figure 14. Significant modulations in LFP power during shifted landmark trials relative to no landmark trials. (A-I) LFP time-frequency spectrograms averaged across all shifted landmark (ShL) trials recorded in monkey V's medial intraparietal sulcus (MIP) (A-C), lateral intraparietal sulcus (LIP) (D,E), and ventral intraparietal sulcus (VIP) (F-H), aligned to the target flash (Tf) (column 1), hand onset (Ho) (column 2), and hand touch (HT) task events (column 3). LFP power spectra displays significant modulations in activity recorded during ShL trials during each task event relative to activity during the same events recorded throughout no landmark (NL) trials. (I,J) LFP time-frequency spectrograms averaged across all ShL trials recorded in monkey L's MIP (I, J) and LIP (K), aligned to Ho (column 2) and HT task events (column 3). LFP power spectra displays significant modulations in activity recorded during ShL trials during each task event relative to activity during the same events recorded throughout NL trials. All task events (Tf, Ho, and Ht) are aligned to time 0.

In summary, there were a wide range of spectral differences between Landmark and NL data across all IPS sites in both monkeys, but no significant difference between SL and ShL. The most consistent difference in LFP activity seemed to be a strong decrease in high-frequency activity during the hand onset and hand touch components of the task, which, importantly, were the two periods associated with motor disinhibition. Activity in the LIP during the target flash event was either minimally significant during landmark trials relative to NL trials, or not significant at all. However, activity in the MIP in both animals and the VIP in monkey V during the target flash in SL trials vs. NL trials commonly displayed an increase of higher-frequency synchrony.

2.4e Band Specific Power Analysis

Figure 15 summarizes our band-specific results by plotting the power of each band through time, for each animal, IPS area (rows) and temporal alignments (columns), using the combined (NL, SL, ShL) datasets. At a qualitative level, this figure shows increased high-frequency power during the target flash event in the MIP, while the hand onset and hand touch events are generally dominated by increases in lower-

frequency activity in both animals, specifically in the delta frequency band. LFP activity in the LIP in both animals during the target flash period displays a similar increase in high-frequency activity, specifically in the beta band. Again, during the motor periods of the task, low-frequency activity in the delta and theta bands displays sharp increases in both animals, while higher-frequency activity is relatively suppressed. This low-frequency activity steadily increases during the hand-onset period and peaks during the hand-touch in both animals. Finally, band-specific activity in monkey V's VIP during the target flash event was characterized by suppressed low-frequency activity, although spectral activity in the beta band displayed a decrease throughout the target flash and into our 300 ms analysis window, before sharply rising towards the end of the window, and finally sharply dropping again. During the motor periods of the task, activity in the VIP again displayed a sharp increase in delta-frequency activity, while spectral activity in the theta, alpha, and beta bands was generally suppressed before strongly increasing in activity post-hand-touch (Figure 15).

To quantify the results of our time-frequency plots, we computed the means of each frequency band during the target flash, hand onset, and hand touch events, and computed a two-way factorial ANOVA to elucidate which bands significantly differed in activity during SL vs. NL trials, as well as ShL vs. NL trials. The analysis windows that we used are indicated by the vertical grey zones shown in Figure 15. For the target flash event, we computed the mean of frequency bands over a period of 300 ms, within a range of 100 to 400 ms post-target flash, as the visual signal of the target would take approximately 100 ms to reach the brain (Figure 15). For the hand onset and touch events, we computed the mean of frequency bands within a 300 ms window, beginning

200 ms before the beginning of the hand movement and ending 100 ms post-hand onset/touch (Figure 15).

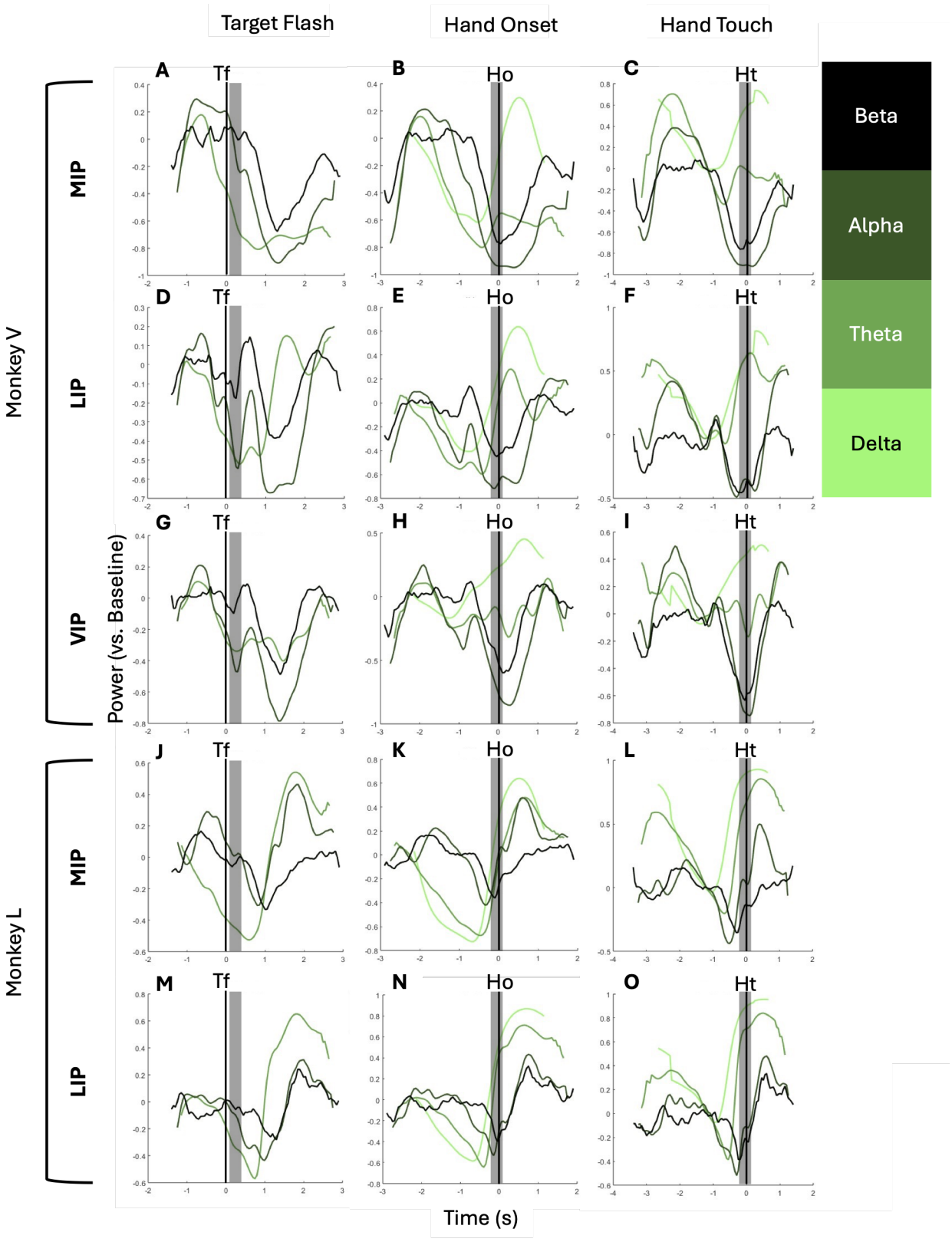

Figure 15. LFP power decomposed into frequency bands. LFP oscillatory power decomposed into frequency bands δ (1-4 Hz), θ (4-8 Hz), α (8-12 Hz), and β (13-30 Hz) for monkey V's medial (MIP; A-C), lateral (LIP; row D-F), and ventral (VIP; row G-I)

intraparietal sulcus, aligned to target flash (Tf; column 1), hand onset (Ho; column 2), and hand touch (Ht; column 3). All task events (Tf, Ho, Ht) occur at time 0, and the grey bars indicate the 300 ms window of where each frequency band mean was computes. LFP oscillatory power decomposed into frequency bands δ (1-4 Hz), θ (4-8 Hz), α (8-12 Hz), and β (13-30 Hz) for monkey L's MIP (J-L) and LIP (M-O), aligned to Tf (column 1), Ho (column 2), and Ht (column 3). All task events (Tf, Ho, Ht) occur at time 0, and the grey bars indicate the 300 ms window of where each frequency band mean was computes.

A series of two-way ANOVAs were conducted to investigate spectral differences in the delta, theta, alpha, and beta frequency bands during each time event window (target flash, 300 ms; hand onset, 300 ms; and hand touch, 300 ms). Significant differences in activity between areas (MIP, LIP, VIP) were observed in both monkeys, while significant differences between experimental conditions (NL, SL, ShL) were only observed in monkey V. These are described below for the target flash, hand onset, and touch events.

TARGET FLASH. First, we compare different areas, bands and tasks during the response period to the target flash (Figure 16, 17). During the target flash event, delta band analysis for monkey V revealed both significant main effects of area, $F(2,4) = 55.31$, $p < .005$, $\eta p^2 = .965$ and condition, $F(2,4) = 15.23$, $p = .01$, $\eta p^2 = .884$. Post hoc analysis for the main effect of area revealed decreased delta frequency in the VIP relative to the MIP ($p = 0.04$) and LIP ($p = .01$) (Figure 16A), while post-hoc analysis for condition revealed greater delta activity in NL trials relative to SL trials ($p = .01$) and ShL trials ($p = .02$) (Figure 17A) but not SL vs. ShL trials ($p = .96$). Analysis of the beta frequency band also revealed a significant main effect of area, $F(2,4) = 55.81$, $p < .001$, $\eta p^2 = .965$, with greater beta activation in the MIP relative to the LIP ($p = <.05$) and VIP ($p = <.001$) (Figure 16D). During the same event, there was a significant main effect of area for the delta band for monkey L, $F(1, 2) = 115.6$, $p = .008$, $\eta p^2 = .983$, with post hoc analysis displaying greater activity in the delta band in the LIP relative to the MIP ($p <.001$); along with the

theta band, $F(1, 2) = 2115.7$, $p < .001$, $\eta p^2 = .999$, such that there was significantly greater theta activity in the LIP relative to the MIP ($p < .001$); alpha band, $F(1,2) = 207.52$, $p < .005$, $\eta p^2 = 0.990$ such that that was significantly greater alpha activity in the MIP relative to the LIP; and beta band, $F(1,2) = 1423.13$, $p < .001$, $\eta p^2 = 0.999$, such that there was significantly greater beta activity in the MIP compared to the LIP ($p < .001$) (Figure 16E-H). In summary, we observed significant increases in delta and beta activity in the MIP and LIP relative to the VIP during the target flash event in monkey V, while in monkey L, I observed significant increases in alpha and beta activity in the MIP relative to the LIP, along with increases in delta and theta activity in the LIP relative to the MIP (Figure 16). Furthermore, we observed an increase in delta activity in NL trials relative to SL trials, as well as NL trials relative to ShL trials only in monkey V and not monkey L.

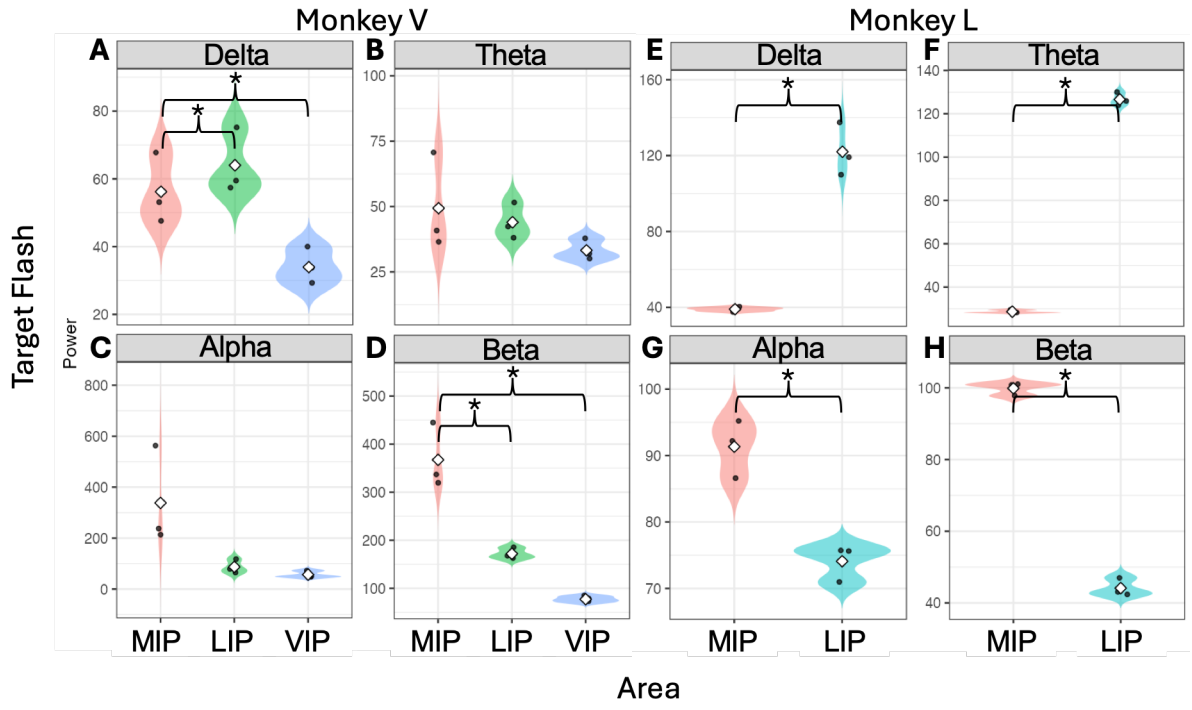

Figure 16. Modulations in frequency-band activity between areas during target flash event. (A-D) This figure displays differences in mean delta, theta, alpha, and beta frequency between intraparietal sulcus (IPS) sites (medial intraparietal sulcus (MIP),

lateral intraparietal sulcus, (LIP), and ventral intraparietal sulcus (VIP)) for monkey V across experimental conditions. (E-H) This figure displays differences in mean delta, theta, alpha, and beta frequency between IPS sites (MIP and LIP) for monkey L across experimental conditions. Asterisks denote statistical significance.

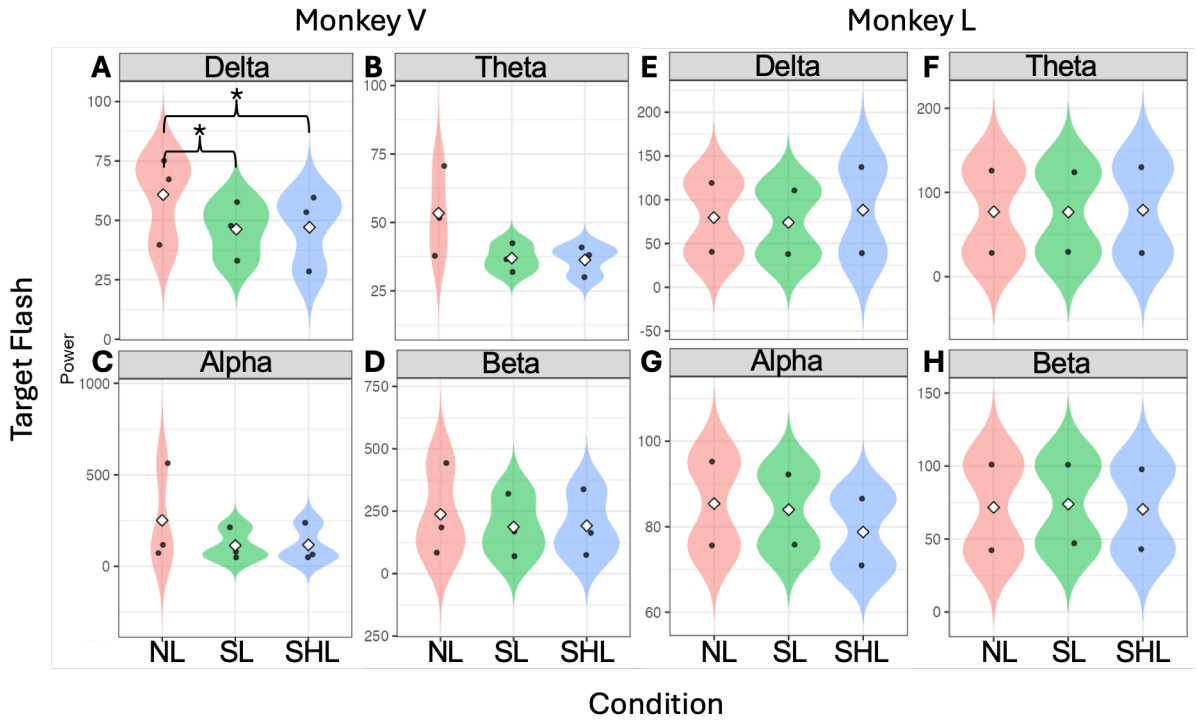

Figure 17. Modulations in frequency-band activity between experimental conditions during target flash event. (A-D) This figure displays differences in mean delta, theta, alpha, and beta frequency between experimental conditions (no landmark (NL), stable landmark (SL), and shifted landmark (ShL)) for monkey V across intraparietal sulcus (IPS) areas. (E-H) This figure displays differences in mean delta, theta, alpha, and beta frequency between experimental conditions (no landmark (NL), stable landmark (SL), and shifted landmark (ShL)) for monkey L across IPS areas. Asterisks denote statistical significance.

HAND ONSET. During the hand onset event (Figures 18, 19) for monkey V, there was a significant main effect of area for the delta band, $F(2,4) = 11.78$, $p < .02$, $\eta p^2 = .855$, such that delta activity was increased in the LIP relative to the VIP ($p = .005$); theta band, $F(2,4) = 16.22$, $p < .01$ $\eta p^2 = .890$, such that theta activity was increased in the LIP relative to the VIP ($p = .01$); alpha band, $F(2,4) = 13.95$, $p = .02$, $\eta p^2 = .875$, such that, again, alpha activity was higher in the LIP compared to the VIP ($p = .02$); and beta band,

$F(2,4) = 74.82$, $p < .001$, $\eta p^2 = .974$, such that there was greater beta activity in the LIP relative to the VIP ($p = .03$) (Figure 18A-D). Furthermore, there was also a significant main effect of condition for the beta band, $F(2,4) = 3158$, $p < .005$, $\eta p^2 = .940$. Post-hoc analysis revealed significant differences in beta activity between NL vs. SL ($p < .005$) and NL vs. ShL trials ($p < .01$), but not SL vs. ShL trials across areas (Figure 19D). During the hand onset event in monkey L, delta band analysis revealed a significant main effect of area, $F(1, 2) = 35.06$, $p = .03$, $\eta p^2 = .946$, such that there was increased activation in the LIP compared to the MIP ($p = .004$). Theta band analysis also revealed a significant main effect of area, $F(1, 2) = 24.40$, $p = .04$, $\eta p^2 = .924$, such that, again, there was increased theta band activity in the LIP compared to the MIP ($p = .01$) (Figure 18E, F). In summary, we again observed increases in MIP and LIP activity across the range of frequency bands relative to VIP activity in monkey V, along with a similar increase of low-frequency activity in the LIP relative to the MIP for monkey L during the hand-onset component of the task. Additionally, we only observed increased beta activity in the NL trials relative to SL and ShL trials in monkey V, with other significant differences between conditions in either monkey.

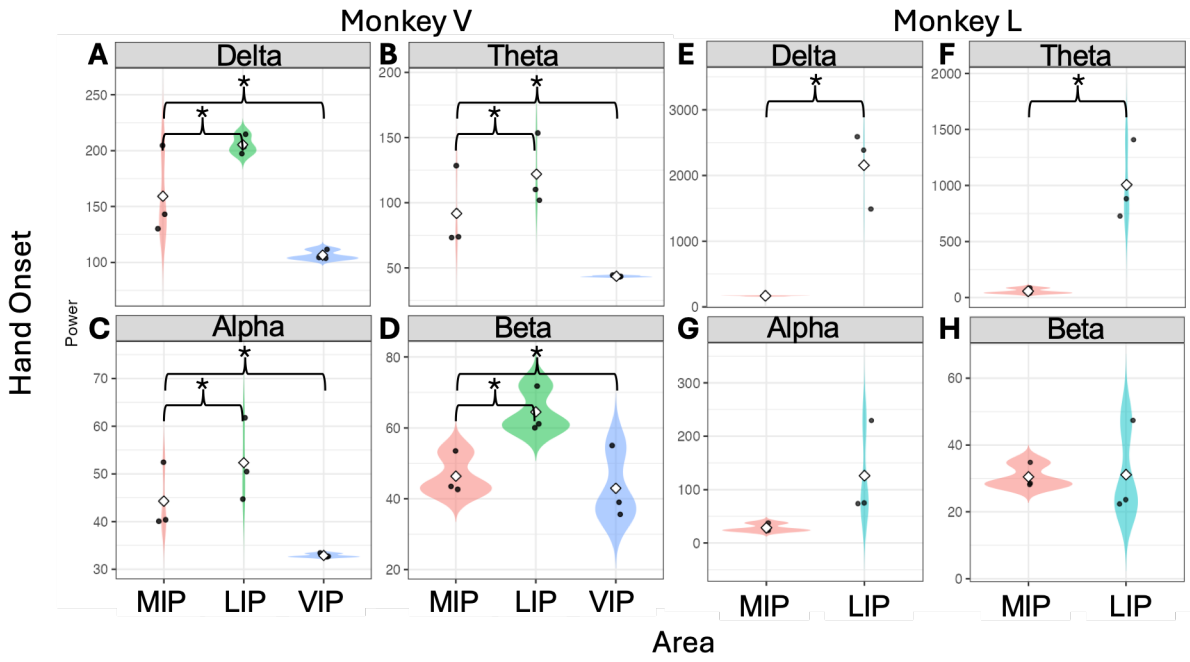

Figure 18. Modulations in frequency-band activity between areas during hand onset event. (A-D) This figure displays differences in mean delta, theta, alpha, and beta frequency between intraparietal sulcus (IPS) sites (medial intraparietal sulcus (MIP), lateral intraparietal sulcus, (LIP), and ventral intraparietal sulcus (VIP)) for monkey V across experimental conditions. (E-H) This figure displays differences in mean delta, theta, alpha, and beta frequency between IPS sites (MIP and LIP) for monkey L across experimental conditions. Asterisks denote statistical significance.

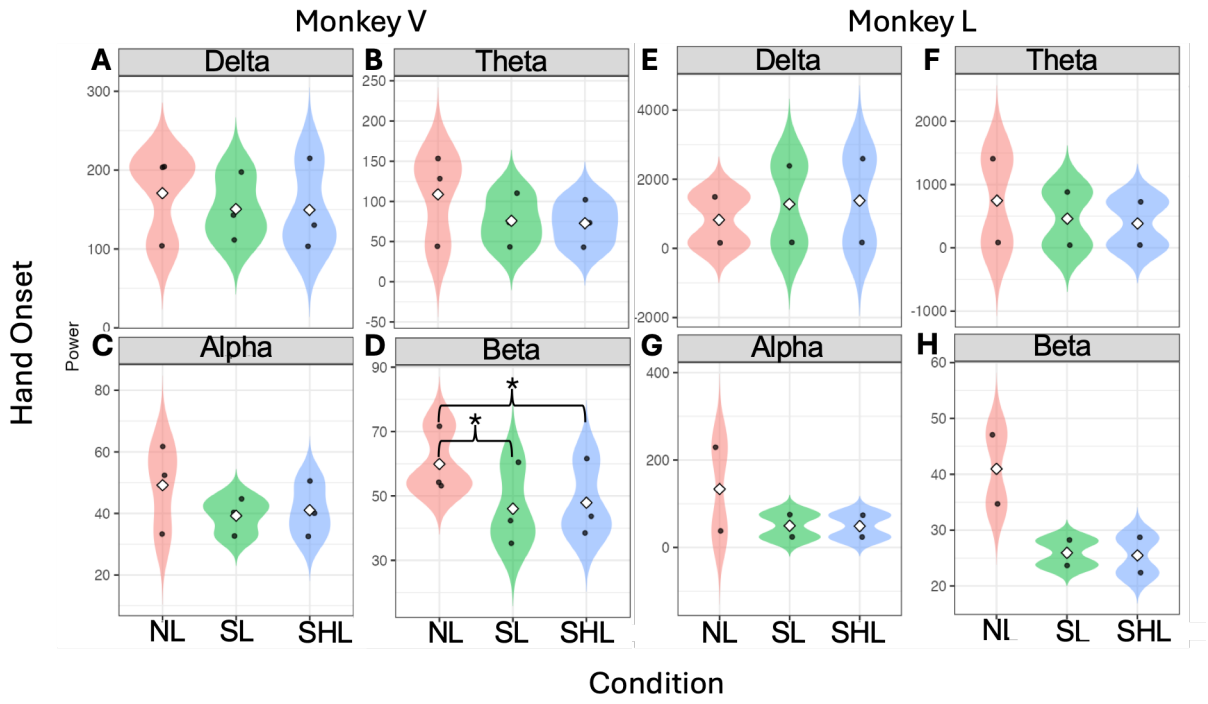

Figure 19. Modulations in frequency-band activity between experimental conditions during hand onset event. (A-D) This figure displays differences in mean delta, theta, alpha, and beta frequency between experimental conditions (no landmark (NL), stable landmark (SL), and shifted landmark (ShL)) for monkey V across intraparietal sulcus (IPS) areas. (E-H) This figure displays differences in mean delta, theta, alpha, and beta frequency between experimental conditions (no landmark (NL), stable landmark (SL), and shifted landmark (ShL)) for monkey L across IPS areas. Asterisks denote statistical significance.

HAND TOUCH. During the hand touch event (Figures 20, 21) for monkey V, analysis of the delta frequency band revealed a significant main effect of area, $F(2,4) = 21.34$, $p = .007$, $\eta p^2 = .914$, such that there was decreased delta activity in the MIP ($p = .02$) and the VIP ($p < .001$) relative to the LIP ($p = .02$), but increased MIP activity compared to the VIP (.01); there was also a significant main effect of area for the theta band, $F(2,4) = 16.51$, $p = .011$, $\eta p^2 = .892$, such that there was increased theta activity in the LIP relative to the VIP ($p = .01$); alpha band, $F(2,4) = 13.05$, $p = .017$, $\eta p^2 = .867$, such that, again, there was increased alpha activity in the LIP relative to the VIP ($p = .02$) (Figure 20A-C); and finally, beta band, which did not reveal a main effect of area, but did

reveal a main effect of condition $F(2,4) = 17.60$, $p = .01$, $\eta p^2 = .900$. Post-hoc comparisons revealed significant differences between NL vs. SL ($p = .01$) and NL vs. ShL trials ($p = .01$), but not SL vs. ShL trials ($p = .22$) (Figure 20D). During the hand touch event in monkey L, only theta band analysis revealed a main effect of area, $F(1, 2) = 219.48$, $p < .005$, $\eta p^2 = .991$, such that there was increased activity in the LIP compared to the MIP ($p < .001$) (Figure 20F). No other significant differences between areas or experimental conditions occurred in any of the task events in either monkey. In summary, we observed increased delta activity in the LIP relative to activity in the MIP and VIP, along with increased delta activity in the MIP relative to the VIP in monkey V. Additionally, we observed increased theta and alpha activity in the LIP relative to the VIP in the same monkey, while we only observed significantly increased theta activity in the LIP compared to the MIP in monkey L. Finally, we again only observed increased beta activity between NL vs. SL and ShL trials in monkey V, with no significant differences between experimental conditions in monkey L.

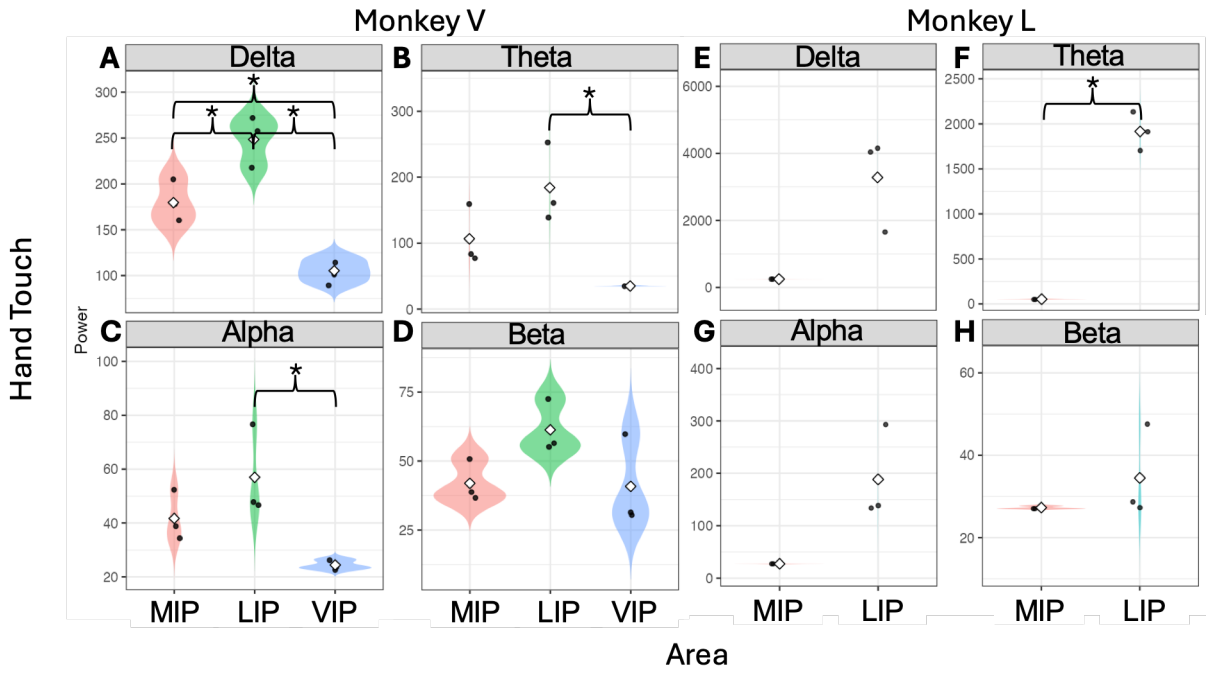

Figure 20. Modulations in frequency-band activity between areas during hand touch event. (A-D) This figure displays differences in mean delta, theta, alpha, and beta frequency between intraparietal sulcus (IPS) sites (medial intraparietal sulcus (MIP), lateral intraparietal sulcus, (LIP), and ventral intraparietal sulcus (VIP)) for monkey V across experimental conditions. (E-H) This figure displays differences in mean delta, theta, alpha, and beta frequency between IPS sites (MIP and LIP) for monkey L across experimental conditions. Asterisks denote statistical significance.

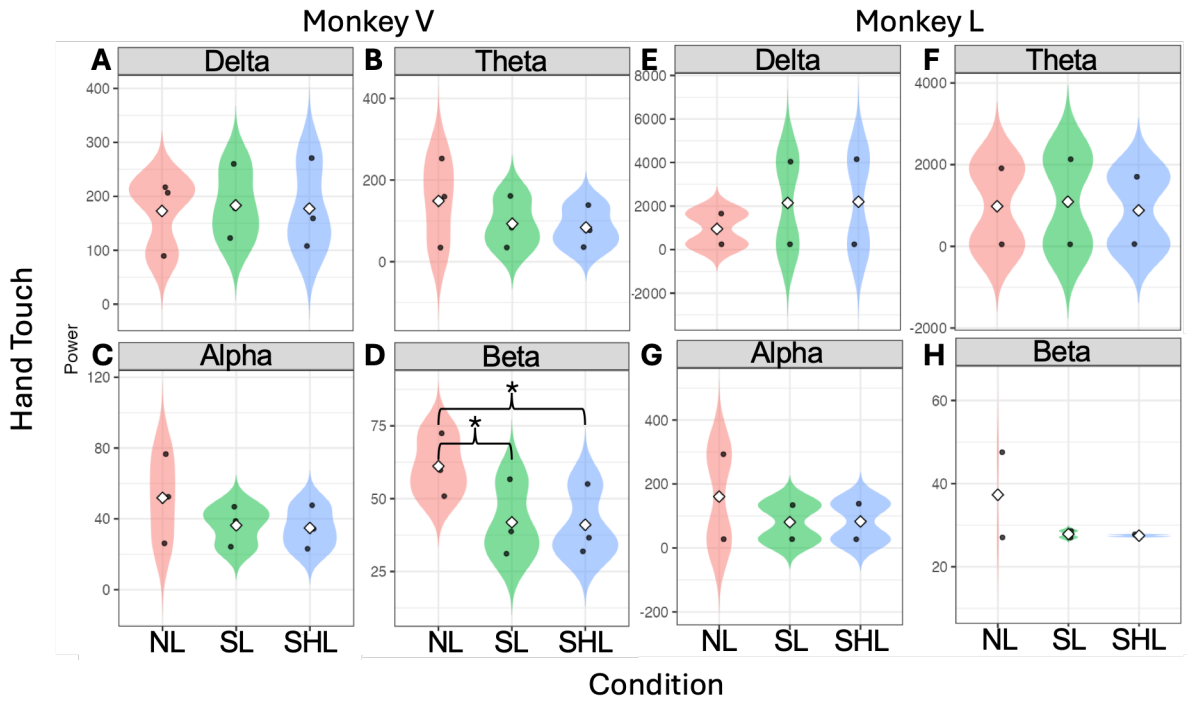

Figure 21. Modulations in frequency-band activity between experimental conditions during hand touch event. (A-D) This figure displays differences in mean delta, theta, alpha, and beta frequency between experimental conditions (no landmark (NL), stable landmark (SL), and shifted landmark (ShL)) for monkey V across intraparietal sulcus (IPS) areas. (E-H) This figure displays differences in mean delta, theta, alpha, and beta frequency between experimental conditions (no landmark (NL), stable landmark (SL), and shifted landmark (ShL)) for monkey L across IPS areas. Asterisks denote statistical significance.

2.5 Discussion

The purpose of this current study was to investigate the effect of reliable and unreliable allocentric visual cues on LFP power recorded from the IPS from two monkeys completing a memory-guided reach task. Based on our initial examination of power relative to baseline, both animals displayed significant and general increases in LFP oscillatory power across the entire spectrum of frequency bands in the LIP during NL trials relative to baseline activity. However, the patterns differed in both animal's MIP – although it was significantly modulated during NL trials relative to baseline activity, we observed an

increase in spectral activity in monkey L's MIP, but a substantial decrease in activity in monkey V's MIP and VIP. Thus, our first hypothesis was supported, as we did observe that oscillatory power during NL trials of the task did significantly differ from LFP power during rest. These patterns in both animals persisted into the SL and ShL vs. NL contrasts, such that the presence of allocentric information modulated LFP oscillatory power during landmark trials relative to NL trials. During SL and ShL trials, both monkeys displayed a significant increase of spectral activity in the LIP relative to NL trials. Once again, we observed differences in MIP activity between animals, such that activity during landmark trials relative to NL trials was associated with a broad increase of power in monkey L's MIP, while landmark trials relative to NL trials were instead associated with significant high-frequency desynchrony in monkey V's MIP and VIP.

When we examined the LFP data using an ANOVA approach rather than a cluster-based approach, we observed that the only significant modulations between experimental conditions occurred in the delta and beta frequency bands, and were observed only for monkey V, and not monkey L. Thus, our second hypothesis was supported by our cluster-based analysis, which displayed that, during recordings from both monkeys, SL and ShL trials did modulate power relative to NL trials. However, our ANOVA results only partially confirmed our second hypothesis, as we only observed modulations in delta and beta LFP power during SL and ShL trials relative to NL trials, with no significant differences between experimental conditions being reported in monkey L. However, it should be noted that cluster-corrected analyses and ANOVA results do commonly differ. Interestingly, in both monkeys and across all areas in the IPS, the SL vs. ShL contrast was never significant, which, unfortunately, did not confirm our third hypothesis. Finally,

we did observe significant differences in spectral activity between areas in both animals (LIP, MIP, and VIP for monkey V; and LIP and MIP for monkey L). During the target flash event, both monkeys displayed significantly greater delta activity in the LIP relative to the MIP along with significantly greater beta activity in the MIP relative to the LIP. Monkey V also displayed increased delta and beta activity in the MIP relative to the VIP, and monkey L displayed increased theta and decreased alpha activity in the MIP vs. the LIP. During the hand onset event, both monkeys displayed greater delta and theta activity in the LIP relative to the MIP**.** Monkey V also displayed an increase in power in the delta, theta, alpha, and beta bands in the MIP compared to the VIP. During the hand touch event, both monkeys displayed increased theta activity in the LIP relative to the MIP, with monkey V displaying increased delta activity in the MIP relative to both LIP and VIP, along with increased alpha activity in the LIP compared to the VIP.

2.5a Behavioural Differences in our Three Tasks

Briefly, our behavioural results for monkey L displayed that gaze onset, hand onset, and completion-to-reach times were shortest for the SL condition, while the mean horizontal reach error increased as the targets moved towards the left side of the screen, i.e., away from the monkey's dominant hand (Lin et al., 2024). Gaze and reach onset times in the NL condition were substantially longer than the SL condition. During the ShL condition, we observed that reaches were pulled in the direction of the final shifted landmark, such that the corresponding allocentric weight was 29%. Additionally, we observed an increase in weight when the landmark was located closer in proximity to the initial gaze position (Lin et al., 2024).

2.5b LFP Modulations During Memory-Guided Reach

Both animals displayed significant LFP power relative to baseline during the memory-guided reach task. A previous study recording LFPs from monkeys performing a memory-guided reaching task observed that task-related LFP modulations seemed to be most prominent in the 12-30 Hz range, a finding that our data supported (Mooshagian et al., 2021). Curiously, the cluster-corrected analysis displayed opposite patterns of beta activity during the task between animals, with monkey L displaying a prominent increase in high-frequency synchrony, and monkey V displaying a pattern of high-frequency desynchrony during the hand onset and hand touch periods of the task. In many studies reporting LFP signals recorded during reaching behaviours in macaques, there is a common peri-movement beta event-related desynchrony (ERD), which occurs prior to, during, and after the motor aspects of the task (Hwang & Anderson, 2009; Lehmann & Scherberger, 2015; Martinez-Vasquez & Gail, 2018; Mooshagian et al., 2021; Mooshagian & Snyder, 2026; Stetson & Anderson, 2014). To that end, our study reports a prominent beta ERD just prior to, during, and just following the reach in monkey V.

However, the question remains to be answered: what *specifically* does beta activity in this context represent, and why does it differ between the two monkeys? First, both monkeys displayed high-frequency activity in the LIP, during both hand onset and hand touch components of the task. The LIP has been strongly associated with saccade-related activity (Roitman & Shadlen, 2002). Previous work investigating the role of the LIP in visually-guided saccade tasks has reported a decrease in beta activity during the motor preparatory period (Chen et al., 2014). With the strong role of the macaque LIP in the coordination of saccades towards a salient target, the high-frequency activity that we

observed in the LIP of both monkeys specifically during the motor periods of the task likely reflects gaze being disinhibited from the fixation dot, as the monkey is now able to saccade freely.

Beta activity in the MIP is more puzzling, as both monkeys showed similar beta intensity, but with a reversed pattern of synchrony during the motor movements of the task. The MIP is an area that is strongly associated with motor planning and execution, especially during memory-guided reaching behaviours (Bakola et al., 2017; Caspers et al., 2012; Grefkes & Fink, 2005). Yet again, previous work has indicated that the LFP signal prior to and during reaching movements is dominated by beta desynchrony, which is exactly the same pattern that we observed in monkey V. However, the difference in beta activity between both animals' LFP signals recorded from their respective MIP's remains a puzzling finding.

The difference in beta power in the MIP between monkey L and V could reflect a difference in motor plans or strategies to complete the task that each monkey may have utilized. For example, Nougaret and colleagues (2024) reported that lower-frequency beta was most associated with quicker reaction times during a reaching task, but was uncorrelated with un-instructed, misadjustments that the animal made during the task. Conversely, high-beta power was unassociated with reaction time, but was more correlated with the anticipation of visual cues, suggesting that different aspects of beta-power are associated with different task demands.

Although we were not able to record VIP activity in monkey L, VIP activity in monkey V was very similar to MIP activity during the reaching task, such that the signal was primarily dominated by beta desynchrony during the motor aspects of the task. VIP

neurons are less associated with strictly motor coordination and execution, and constitute more of a polymodal zone for a variety of sensory information, including visual, tactile, and auditory information (Grefkes & Fink, 2005). VIP neurons have been shown to discharge when a target appears in the animal's periphery, which could explain why we observed increased VIP activity during the target flash period. Furthermore, neurons in the VIP are associated with the integration of multiple senses to coordinate accurate self-motion towards a target. Although the animals in our study were fairly restricted, and could only utilize their right arm to interact with the touch screen, the VIP activation could perhaps reflect the coordination of visual and proprioceptive information to guide the arm accurately through the dark to the screen (Bremmer et al., 2002). However, the role of the VIP in this task is not as clear as the MIP, for example. Prior work has shown that the VIP is also strongly associated with defensive movements that the monkey would encounter in the wild, and likely would not encounter during a rather innocuous reaching task (Cook et al., 2003; Grefkes & Fink, 2005). In the context of our memory-guided reach task, beta desynchrony during the hand onset and hand touch components of the task could reflect the integration of multisensory information to coordinate attention towards the remembered target location.

2.5c LFP Modulations Associated with Allocentric Visual Information

In monkeys L and V, we reported significant differences in LFP power during SL trials relative to NL trials, as well as ShL trials relative to NL trials. We did not observe any significant differences in LFP activation during SL trials relative to ShL trials, suggesting that the LFP signal from both monkeys was able to discriminate between NL vs. SL and ShL trials, but not SL vs. ShL trials.

Although the IPS is a predominantly egocentric site, previous studies have reported that allocentric information has modulated the activity of neurons in this area. For example, Taghizadeh and colleagues (2024) exposed monkeys to a reach task in the presence of landmarks, and observed that neurons along the dorsal stream encoded allocentric information. Additionally, they also reported that the presence of a landmark during the reaching task substantially modulated the LFP signal, indicating that the shifting between visual reference frames may be an ongoing and dynamic process. There is currently a paucity in the number of studies that specifically focus on LFP power recorded from the macaque IPS during egocentric vs. allocentric reaching, but the pattern of results from this present study provide support for the IPS's role in encoding the presence of landmarks during memory-guided reaching behaviour.

However, when we examined the results of our ANOVA, we observed that the only significant differences in activation between SL and ShL trials vs. NL trials occurred only in the delta and beta bands, with no significant differences being observed in the theta or alpha bands. Additionally, we only observed these results in monkey V, and not monkey L. Although these results remain puzzling, they are nonetheless consistent with delta and beta band activity during reaching tasks reported in previous literature. For example, prior studies have consistently observed increases in delta power before the actual movement onset, which is similar to our observation of increased delta power during the target-flash task event (Saleh et al., 2010; Popovych et al., 2016). Specifically, we observed increases in delta power during the target flash event when comparing SL and ShL trials to NL trials, which is a finding that has not yet been reported in the current body of literature. Sabra and colleagues (2019) observed an increase in delta band power associated with seen

and attended visual categories. During landmark (SL and ShL) trials, there is a greater amount of visual information on-screen that must be attenuated to. Thus, the increased delta signal during the target flash event of the task could perhaps be associated with greater visual attentional demands.

Additionally, we also observed a difference in beta power during SL and ShL trials relative to NL trials in our ANOVA results during the hand onset and hand touch periods of the task, a finding that is aligned with prior studies observing suppressed beta power aligned with reaching movements to a salient target (Mooshagian et al., 2021; Scherberger et al., 2005). In the context of our study, the significant suppression of beta activity observed during the hand onset and hand touch events in SL and ShL trials relative to NL trials may reflect reduced uncertainty in the internal representation of the target location. The presence of stable landmarks likely provides an additional spatial reference frame that facilitates the maintenance and transformation of the visuospatial target representation into a motor command. Consequently, less computational demand may be placed on maintaining and updating the target representation, resulting in a more pronounced suppression of beta activity during the hand onset and hand touch periods.

2.5d Stable Landmark Vs. Shifted Landmark Trials

We did not find any significant differences for the SL vs. ShL contrast, across both animals and all recorded areas within the IPS. Puzzlingly, our behavioural results reported in Lin et al. (2024) showed that gaze endpoints did shift towards the direction of the landmark shift, despite our LFP data finding no significant differences between SL and ShL trials. There are a few explanations for this null finding. First, it is likely that the LFP signal may have been too slow to pick up on such a quick, surreptitious shift of the

landmark. Mooshagian et al. (2021) reported that LFP signals generally lag behind single-unit spikes by approximately 125 ms. As LFPs integrate and average the signal of local populations of neurons, the landmark shift may instead be integrated in a more fine-grained manner that may have been missed by the inherent nature of LFP recordings.

Second, it is likely that neurons along the IPS may encode the presence of allocentric visual cues (i.e., a landmark), but are nonetheless invariant as to whether that cue is reliable or not. Bharmauria et al. (2020) reported that neurons in the frontal cortex encoded the landmark shift. Therefore, it is likely that the mechanisms supporting SL/ShL discrimination occur upstream in the frontal cortex, rather than in parietal areas. Furthermore, Hwang & Anderson (2009) determined that LFPs recorded from the macaque PRR are better at discriminating behavioural states during a reaching task (such as plan vs. execution), rather than discriminating between fine-grained sensory input, such as a surreptitious landmark shift.

Lastly, Lehmann & Scherberger (2015) reported that LFPs recorded from macaque parietal areas encode spatial information in a consistent manner across task epochs. Since we found the greatest activation during the hand onset and hand touch motor periods of the task, it could be likely that the landmark shift during the late mask period could have occurred too late in the task to pick up on neurophysiological differences. In other words, the monkey may have already formed a concrete motor plan by the time that the landmark underwent a shift, and the LFP signal may have been too slow to pick up on the fine-grained alterations in the motor plan that may have occurred as a result of observing the shift.

2.5e Overall Differences Between LIP, MIP, and VIP

Our observation that there were significant differences in spectral activity between areas in monkey V (MIP, LIP, and VIP) and monkey L (MIP and LIP) is aligned with previous literature reporting functional distinctions between banks in visuomotor control (Grefkes & Fink, 2005). Generally, during the target flash event, there was significantly greater delta activity in the LIP relative to all other areas for both monkeys, however, there was significantly greater high-frequency activity (alpha and beta) in the MIP relative to the LIP. During the hand onset event, there was a similar pattern of increased spectral activity in the LIP relative to all other areas in both animals, which persisted into the hand touch event, where activity in the LIP was significantly stronger than the other IPS banks in both animals. Increased activity in the LIP relative to all other areas is not a surprising finding. The LIP is widely associated with multiple aspects of visuomotor control, to an arguably much larger extent than its neighbouring banks. For example, previous work has reported neuronal responses in the LIP associated with visual stimulus detection, along with the subsequent memory delay, along with the saccadic response towards the remembered target location (Gnadt & Andersen, 1988). Additionally, LIP neurons do not just encode saccades. Instead, Dean and colleagues (2011) reported that neurons along the LIP encoded predictive reaction times of reach-saccade movements, but not saccades independent of an arm reach.

2.6 Conclusion

The LFP activity that we recorded from the IPS of two monkeys performing a memory-guided reach task displayed that the presence of a landmark significantly modulated neuronal activity across the lateral, medial, and ventral banks of the IPS.

However, a series of two-way ANOVAs only revealed significant differences between egocentric vs. allocentric trials in monkey V, but not monkey L. Specifically, only delta and beta frequency bands were found to significantly differ during SL and ShL trials relative to NL trials in monkey V. Through this study, we have provided data that supports prior work indicating that neurons along the IPS respond to allocentric information during memory-guided reaching behaviours. However, when we took a closer look at the differences in frequency band activity during the different components of the task, we observed that monkey V, and not monkey L, displayed significant modulation only in the delta and beta bands during SL/ShL vs. NL comparisons. While the task-related modulations in activity do match what has been reported in macaque electrophysiological literature, these effects were only present in one animal in the ANOVA analysis, indicating that further work should be conducted to fully elucidate the spectral mechanisms behind reaching behaviours in the primate PRR under naturalistic contexts. Although we observed variability in LFP responses between both monkeys, this may reflect inter-subject differences in neural dynamics and task engagement. Future studies should investigate the oscillatory subtleties within the macaque IPS underlying egocentric and allocentric memory-guided reaching behaviours.

CHAPTER 3 GENERAL DISCUSSION

3.0 Discussion

In this chapter, I will discuss how our work has contributed to the broader field of electrophysiological research in macaques on the influence of egocentric and allocentric visual information during reaches to a remembered target. I will also report the

implications of our study and hopeful future directions, along with the limitations with our work.

3.1 Summary and Implications

In this current study, I showed that, in general, the presence of allocentric information during reaching behaviours conducted by monkeys modulated the local activity of neurons along the IPS. The results from our cluster-corrected analysis displayed that, across task events (target flash, hand onset, and hand touch) activity throughout the range of frequency bands (theta-beta) were modulated during NL vs. SL and NL vs. ShL trials, but not SL vs. ShL trials in both monkeys. However, the results from our factorial ANOVA were more complicated, in that monkey L did not display any task-related modulations in LFP activity, while monkey V did, but only in the delta and beta frequency bands. Interestingly, I did not observe any differences in both our cluster-corrected analysis as well as our ANOVA in LFP activity during SL vs. ShL comparisons. Curiously, the results of our two-way ANOVA displayed statistically significant differences in activity in the delta and beta bands during SL and ShL trials relative to NL trials only in monkey V, but not monkey L, despite the latter monkey displaying statistically significant modulations in LFP activity during SL and ShL trials relative to NL trials in our cluster-corrected analysis.

3.2 Clinical Implications

Various neurological and physical conditions can separately affect areas processing egocentric and allocentric information. For example, congenital blindness is associated with predominant deficits in egocentric, rather than allocentric visual

processing (Martolini et al., 2021). Additionally, diseases such as Alzheimer's and Parkinson's disease are associated with major impairments in allocentric processing (Wood et al., 2016; Reinshagen, 2024). Learning about how egocentric and allocentric reference frames are neurologically represented is an important step in the creation of diagnostic criteria to better support earlier interventions for age-related diseases. For example, Wood et al. (2016) observed that performance on an allocentric spatial memory task in patients with mild cognitive impairment significantly predicted the onset of a full Alzheimer's diagnosis by an entire year. Additionally, learning about the neurological mechanisms underlying visual spatial coding could also support various prosthesis efforts for the visually impaired. ARGUS II was the first visual cortex prosthesis to be approved by the FDA, and is still under clinical trials. This prosthesis fits the user with a pair of glasses with a camera attached to the front, which transduces visual information into electrical signals which are directly transmitted to the retina to produce rudimentary vision. Other visual prosthesis efforts, such as the Orion cortical visual prosthesis system, aim to restore vision by delivering structured electrical stimulation to the visual cortex via implanted electrode arrays. Thus, progress in understanding visuospatial representations in the parietal cortex, specifically, the mechanisms underlying egocentric and allocentric coding, are critical for furthering the development of neural prosthetics.

3.3 Limitations

Many of the behavioural limitations here were mentioned in Lin et al. (2024). Briefly, I had to ensure that our reward window for correct trials was large enough to include the original and the shifted targets, which, due to the size of the window, prevented us from being able to conduct a purely egocentric/allocentric task. Additionally, our touch screen

recorded the first instance that the animal touched the screen. This may not reflect the monkey's intended response, as I did notice that both monkeys employed two different types of reaching plans toward the screen. For example, monkey L would contact the screen with their entire palm before returning their hand to rest. In contrast, monkey V would not touch the screen with their full hand, instead, they would make initial contact with their index finger, before "scooping" their hand downwards, as if trying to maximize the surface area of their reach. As only the first contact of the monkey's hand with the screen dictates a correct or incorrect response, so this compensatory effect didn't actually increase the animal's probability of touching within the correct response window. However, monkey V did not seem to learn this, as they kept repeating the same strategy for every trial on every recording date.

With respect to additional limitations, I was not able to analyze delta band activity during the task using our cluster-corrected analysis, meaning that I may have missed out on potentially critical information, especially since further analyses reported that delta activity was significantly modulated during SL trials relative to NL trials in monkey V. Furthermore, our cluster-corrected analysis could only compare equal lengths of data, meaning that our target events of interest could only be as long as our baseline time window was. This limitation made it impossible for us to observe differences in LFP activity continuously throughout the entire task, rather, it only offered glimpses into power modulations during small (500 ms) windows.

Furthermore, often our data was very contaminated with electrical noise and artifacts, such that, even following preprocessing, there were many recording dates that could not be included in the analysis. Due to this, I was not able to include many recording

sessions, which unfortunately meant that potentially important recording dates were discarded. Going forward, there should be additional and more robust preprocessing steps to ensure that the LFP data has been completely cleaned of artifacts. Additionally, I was unable to record VIP data in monkey L, due to unintentionally installing a chamber that was too large to permit the electrode access to such a deep area. Finally, I observed many differences between our cluster-corrected analysis and ANOVA analysis. Divergences between cluster-based and ANOVA results likely reflect differences in sensitivity to temporally and spectrally localized effects. While ANOVAs test mean differences within predefined windows, cluster-based analyses are sensitive to structured effects distributed across time-frequency space, which may not be preserved after temporal averaging. Generally, it is normal to observe differences between both types of analyses, however, our differences in results made interpreting the true underlying spectral mechanisms behind reaching behaviour difficult to interpret.

3.4 Future directions

Here, I showed that in general, the presence of allocentric information during a memory-guided cue conflict task in macaques modulated LFP activity recorded in the IPS, which yielded a massive dataset. For the future, there are several next steps that should be taken to fully explore the intricacies hidden within. Analyzing cross-frequency coupling is a natural extension of our work. Although not included in the present study, cross-frequency coupling has been implicated in motor planning, working memory, and attentional control, and may provide insight into interactions between neural processes operating at different temporal scales that are not directly observable from band-limited power estimates. We also collected spiking activity, which could be important for parsing

out some modulations in activity that LFP's may have missed. The memory-guided reach task unfolds over relatively short time scales, and while LFPs reflect population-level synaptic activity, they do not directly resolve spike timing or neuron-specific coding dynamics. Furthermore, we have already completed building a classifier model, which was trained on the LFP data to classify the experimental task associated with each trial – for example, it was trained to decode whether a certain trial represented a NL, SL, or ShL task to a very high degree of accuracy. We are also in the process of training another computational model on NL, SL, and ShL trials of the same task, to see if we can virtually replicate the behaviour that was reported previously (Lin et al., 2024).

REFERENCES

Ahmed, B., Ko, H., Rüsseler, M., Smith, J. E., & Krug, K. (2025). Anatomical circuits for flexible spatial mapping by single neurons in posterior parietal cortex. *Communications Biology*, *8*(1). https://doi.org/10.1038/s42003-025-08596-6

Andersen, R. A., & Buneo, C. A. (2002). Intentional maps in posterior parietal cortex. *Annual Review of Neuroscience*, *25*(1), 189–220. https://doi.org/10.1146/annurev.neuro.25.112701.142922

Bakola, S., Passarelli, L., Huynh, T., Impieri, D., Worthy, K. H., Fattori, P., Galletti, C., Burman, K. J., & Rosa, M. G. (2017a). Cortical afferents and myeloarchitecture distinguish the medial intraparietal area (MIP) from neighboring subdivisions of the macaque cortex. *Eneuro*, *4*(6). https://doi.org/10.1523/eneuro.0344-17.2017

Bakola, S., Passarelli, L., Huynh, T., Impieri, D., Worthy, K. H., Fattori, P., Galletti, C., Burman, K. J., & Rosa, M. G. (2017b). Cortical afferents and myeloarchitecture distinguish the medial intraparietal area (MIP) from neighboring subdivisions of the macaque cortex. *Eneuro*, *4*(6). https://doi.org/10.1523/eneuro.0344-17.2017

Batista, A. P., Buneo, C. A., Snyder, L. H., & Andersen, R. A. (1999a). Reach plans in eye-centered coordinates. *Science*, *285*(5425), 257–260. https://doi.org/10.1126/science.285.5425.257

Batista, A. P., Buneo, C. A., Snyder, L. H., & Andersen, R. A. (1999b). Reach plans in eye-centered coordinates. *Science*, *285*(5425), 257–260. https://doi.org/10.1126/science.285.5425.257

Bharmauria, V., Sajad, A., Li, J., Yan, X., Wang, H., & Crawford, J. D. (2020). Integration of eye-centered and landmark-centered codes in frontal eye field gaze responses. *Cerebral Cortex*, *30*(9), 4995–5013. https://doi.org/10.1093/cercor/bhaa090

Bharmauria, V., Sajad, A., Yan, X., Wang, H., & Crawford, J. D. (2020). Spatiotemporal coding in the macaque supplementary eye fields: Landmark influence in the target-to-gaze transformation. *Eneuro*, *8*(1). https://doi.org/10.1523/eneuro.0446-20.2020

Bharmauria, V., Seo, S., & Crawford, J. D. (2025). Neural integration of egocentric and allocentric visual cues in the gaze system. Journal of Neurophysiology, 133(1), 109–120. https://doi.org/10.1152/jn.00498.2024

Bisley, J. W., & Goldberg, M. E. (2003). Neuronal activity in the lateral intraparietal area and spatial attention. *Science*, *299*(5603), 81–86. https://doi.org/10.1126/science.1077395

Blatt, G. J., Andersen, R. A., & Stoner, G. R. (1990). Visual receptive field organization and cortico-cortical connections of the lateral intraparietal area (area lip) in the macaque. *Journal of Comparative Neurology*, *299*(4), 421–445. https://doi.org/10.1002/cne.902990404

Blohm, G., & Crawford, J. D. (2007). Computations for geometrically accurate visually guided reaching in 3-D space. *Journal of Vision*, *7*(5), 4. https://doi.org/10.1167/7.5.4

Bremmer, F., Kubischik, M., Hoffmann, K.-P., & Krekelberg, B. (2009). Neural dynamics of saccadic suppression. *The Journal of Neuroscience*, *29*(40), 12374–12383. https://doi.org/10.1523/jneurosci.2908-09.2009

Britten, K. H., Shadlen, M. N., Newsome, W. T., & Movshon, J. A. (1993). Responses of neurons in macaque MT to stochastic motion signals. *Visual Neuroscience*, *10*(6), 1157–1169. https://doi.org/10.1017/s0952523800010269

Buneo, C. A., Jarvis, M. R., Batista, A. P., & Andersen, R. A. (2002). Direct visuomotor transformations for reaching. *Nature*, *416*(6881), 632–636. https://doi.org/10.1038/416632a

Byrne P. A., Cappadocia DC, Crawford JD. Interactions between gaze-centered and allocentric representations of reach target location in the presence of spatial updating. Vision Res. 2010 Dec;50(24):2661-70. doi: 10.1016/j.visres.2010.08.038. Epub 2010 Sep 15. PMID: 20816887.

Byrne, P. A., & Crawford, J. D. (2010). Cue reliability and a landmark stability heuristic determine relative weighting between egocentric and allocentric visual information in memory-guided reach. *Journal of Neurophysiology*, *103*(6), 3054–3069. https://doi.org/10.1152/jn.01008.2009

Caspers, S., Amunts, K., & Zilles, K. (2012). Posterior parietal cortex. *The Human Nervous System*, 1036–1055. https://doi.org/10.1016/b978-0-12-374236-0.10028-8

Chambellant, F., Falaki, A., Moreau-Debord, I., French, R., Serrano, E., Quessy, S., Dancause, N., & Thomas, E. (2024). Variations in clustering of multielectrode local field potentials in the motor cortex of macaque monkeys during a reach-and-grasp task. *Eneuro*, *11*(9). https://doi.org/10.1523/eneuro.0047-24.2024

Chen, Y., & Crawford, J. D. (2019). Allocentric representations for target memory and reaching in human cortex. Annals of the New York Academy of Sciences, 1464(1), 142–155. https://doi.org/10.1111/nyas.14261

Chen, M., Wei, L., & Liu, Y. (2014). Motor preparation attenuates neural variability and beta-band LFP in parietal cortex. *Scientific Reports*, *4*(1). https://doi.org/10.1038/srep06809

Chen, Y., Monaco, S., Byrne, P., Yan, X., Henriques, D. Y. P., & Crawford, J. D. (2014). Allocentric versus egocentric representation of remembered reach targets in human cortex. *The Journal of Neuroscience*, *34*(37), 12515–12526. https://doi.org/10.1523/jneurosci.1445-14.2014

Connolly, J. D., Goodale, M. A., Desouza, J. F., Menon, R. S., & Vilis, T. (2000). A comparison of frontoparietal fmri activation during Anti-Saccades and anti-pointing.

Journal of Neurophysiology, *84*(3), 1645–1655. https://doi.org/10.1152/jn.2000.84.3.1645

Cooke, D. F., Taylor, C. S., Moore, T., & Graziano, M. S. (2003). Complex movements evoked by microstimulation of the ventral intraparietal area. *Proceedings of the National Academy of Sciences*, *100*(10), 6163–6168. https://doi.org/10.1073/pnas.1031751100

Crawford, J. D., Medendorp, W. P., & Marotta, J. J. (2004). Spatial transformations for Eye–hand coordination. *Journal of Neurophysiology*, *92*(1), 10–19. https://doi.org/10.1152/jn.00117.2004

Crawford, J. Douglas, Ceylan, M. Z., Klier, E. M., & Guitton, D. (1999). Three-dimensional eye-head coordination during gaze saccades in the Primate. *Journal of Neurophysiology*, *81*(4), 1760–1782. https://doi.org/10.1152/jn.1999.81.4.1760

Culham, J. C., Danckert, S. L., Souza, J. F., Gati, J. S., Menon, R. S., & Goodale, M. A. (2003). Visually guided grasping produces fmri activation in dorsal but not ventral stream brain areas. *Experimental Brain Research*, *153*(2), 180–189. https://doi.org/10.1007/s00221-003-1591-5

Dean, H. L., Hagan, M. A., & Pesaran, B. (2012). Only coherent spiking in posterior parietal cortex coordinates looking and reaching. Neuron, 73(4), 829–841. https://doi.org/10.1016/j.neuron.2011.12.035

De Vitis, M., Breveglieri, R., Hadjidimitrakis, K., Vanduffel, W., Galletti, C., & Fattori, P. (2019). The neglected medial part of macaque area pe: Segregated processing of reach depth and direction. *Brain Structure and Function*, *224*(7), 2537–2557. https://doi.org/10.1007/s00429-019-01923-8

Denker, M., Zehl, L., Kilavik, B. E., Diesmann, M., Brochier, T., Riehle, A., & Grün, S. (2018). LFP beta amplitude is linked to mesoscopic spatio-temporal phase patterns. *Scientific Reports*, *8*(1). https://doi.org/10.1038/s41598-018-22990-7

Esghaei, M., & Daliri, M. R. (2014). Decoding of visual attention from LFP signals of macaque mt. *PLoS ONE*, *9*(6). https://doi.org/10.1371/journal.pone.0100381

Eskandar, E. N., & Assad, J. A. (1999). Dissociation of visual, motor and predictive signals in parietal cortex during visual guidance. *Nature Neuroscience*, *2*(1), 88–93. https://doi.org/10.1038/4594

Eskandar, E. N., & Assad, J. A. (2002). Distinct nature of directional signals among parietal cortical areas during visual guidance. *Journal of Neurophysiology*, *88*(4), 1777–1790. https://doi.org/10.1152/jn.2002.88.4.1777

Fattori, P., Kutz, D. F., Breveglieri, R., Marzocchi, N., & Galletti, C. (2005). Spatial tuning of reaching activity in the medial parieto-occipital cortex (area V6A) of macaque monkey. *European Journal of Neuroscience*, *22*(4), 956–972. https://doi.org/10.1111/j.1460-9568.2005.04288.x

Fiehler, K., & Karimpur, H. (2022). Spatial coding for action across spatial scales. Nature Reviews Psychology, 2(2), 72–84. https://doi.org/10.1038/s44159-022-00140-1

Goodale, M. (1998). Frames of reference for perception and action in the Human Visual System. Neuroscience & Biobehavioral Reviews, 22(2), 161–172. https://doi.org/10.1016/s0149-7634(97)00007-9

Goodale, M. A. (2011). Transforming vision into action. Vision Research, 51(13), 1567–1587. https://doi.org/10.1016/j.visres.2010.07.027

Goodale, M. A., & Milner, A. D. (1992). Separate visual pathways for perception and action. Trends in Neurosciences, 15(1), 20–25. https://doi.org/10.1016/0166-2236(92)90344-8

Gnadt JW, Andersen RA. Memory related motor planning activity in posterior parietal cortex of macaque. Exp Brain Res. 1988;70:216–220. doi: 10.1007/BF00271862.

Grefkes, C., & Fink, G. R. (2005a). Review: The Functional Organization of the intraparietal sulcus in humans and Monkeys. Journal of Anatomy, 207(1), 3–17. https://doi.org/10.1111/j.1469-7580.2005.00426.x

Grefkes, C., & Fink, G. R. (2005b). Review: The Functional Organization of the intraparietal sulcus in humans and Monkeys. Journal of Anatomy, 207(1), 3–17. https://doi.org/10.1111/j.1469-7580.2005.00426.x

Heinrichs-Graham, E., Taylor, B. K., Wang, Y.-P., Stephen, J. M., Calhoun, V. D., & Wilson, T. W. (2020). Parietal oscillatory dynamics mediate developmental improvement in motor performance. *Cerebral Cortex*, *30*(12), 6405–6414. https://doi.org/10.1093/cercor/bhaa199

Heinrichs-Graham, E., & Wilson, T. W. (2015). Coding complexity in the Human Motor Circuit. *Human Brain Mapping*, *36*(12), 5155–5167. https://doi.org/10.1002/hbm.23000

How do we see?. InPsych. (n.d.). https://in-psych.co.uk/2024/05/how-do-we-see/

Huerta, M. F., & Kaas, J. H. (1990). Supplementary eye field as defined by intracortical microstimulation: Connections in macaques. *Journal of Comparative Neurology*, *293*(2), 299–330. https://doi.org/10.1002/cne.902930211

Huerta, M. F., Krubitzer, L. A., & Kaas, J. H. (1987). Frontal eye field as defined by intracortical microstimulation in squirrel monkeys, Owl Monkeys, and Macaque Monkeys II. cortical connections. *Journal of Comparative Neurology*, *265*(3), 332–361. https://doi.org/10.1002/cne.902650304

Hwang, E. J., & Andersen, R. A. (2009). Brain control of movement execution onset using local field potentials in posterior parietal cortex. *The Journal of Neuroscience*, *29*(45), 14363–14370. https://doi.org/10.1523/jneurosci.2081-09.2009

Kaiser, J., Birbaumer, N., & Lutzenberger, W. (2001). Event-related beta desynchronization indicates timing of response selection in a delayed-response

paradigm in humans. *Neuroscience Letters*, *312*(3), 149–152. https://doi.org/10.1016/s0304-3940(01)02217-0

Khayat, P. S., Niebergall, R., & Martinez-Trujillo, J. C. (2010). Frequency-dependent attentional modulation of local field potential signals in Macaque Area MT. *The Journal of Neuroscience*, *30*(20), 7037–7048. https://doi.org/10.1523/jneurosci.0404-10.2010

Kilavik, B. E., Ponce-Alvarez, A., Trachel, R., Confais, J., Takerkart, S., & Riehle, A. (2011). Context-related frequency modulations of macaque motor cortical LFP beta oscillations. *Cerebral Cortex*, *22*(9), 2148–2159. https://doi.org/10.1093/cercor/bhr299

Klier, E. M., Wang, H., & Crawford, J. D. (2003). Three-dimensional eye-head coordination is implemented downstream from the superior colliculus. *Journal of Neurophysiology*, *89*(5), 2839–2853. https://doi.org/10.1152/jn.00763.2002

Krigolson, O., & Heath, M. (2004). Background visual cues and memory-guided reaching. *Human Movement Science*, *23*(6), 861–877. https://doi.org/10.1016/j.humov.2004.10.011

Lafer-Sousa, R., & Conway, B. R. (2013). Parallel, multi-stage processing of colors, faces and shapes in macaque inferior temporal cortex. *Nature Neuroscience*, *16*(12), 1870–1878. https://doi.org/10.1038/nn.3555

Lehmann, S. J., & Scherberger, H. (2015). Spatial representations in local field potential activity of primate anterior intraparietal cortex (AIP). *PLOS ONE*, *10*(11). https://doi.org/10.1371/journal.pone.0142679

Leys, C., Ley, C., Klein, O., Bernard, P., & Licata, L. (2013). Detecting outliers: Do not use standard deviation around the mean, use absolute deviation around the median. *Journal of Experimental Social Psychology*, *49*(4), 764–766. https://doi.org/10.1016/j.jesp.2013.03.013

Li, J., Sajad, A., Marino, R., Yan, X., Sun, S., Wang, H., & Crawford, J. D. (2017). Effect of allocentric landmarks on Primate Gaze Behavior in a cue conflict task. *Journal of Vision*, *17*(5), 20. https://doi.org/10.1167/17.5.20

Lin, J., Wang, H., Sun, S., Yan, X., & Crawford, J. D. (2023a). Influence of a visual landmark shift on memory-guided reaching in Monkeys. *Journal of Vision*, *23*(9), 4828. https://doi.org/10.1167/jov.23.9.4828

Lin, J., Wang, H., Sun, S., Yan, X., & Crawford, J. D. (2023b). Influence of a visual landmark shift on memory-guided reaching in Monkeys. *Journal of Vision*, *23*(9), 4828. https://doi.org/10.1167/jov.23.9.4828

Lu, Z., & Fiehler, K. (2020). Spatial updating of allocentric landmark information in real-time and memory-guided reaching. *Cortex*, *125*, 203–214. https://doi.org/10.1016/j.cortex.2019.12.010

Martínez-Vázquez, P., & Gail, A. (2018). Directed interaction between monkey premotor and posterior parietal cortex during motor-goal retrieval from working memory. *Cerebral Cortex*, *28*(5), 1866–1881. https://doi.org/10.1093/cercor/bhy035

Martolini, C., Cappagli, G., Saligari, E., Gori, M., & Signorini, S. (2021a). Allocentric spatial perception through vision and touch in sighted and Blind Children. Journal of Experimental Child Psychology, 210, 105195. https://doi.org/10.1016/j.jecp.2021.105195

Martolini, C., Cappagli, G., Saligari, E., Gori, M., & Signorini, S. (2021b). Allocentric spatial perception through vision and touch in sighted and Blind Children. Journal of Experimental Child Psychology, 210, 105195. https://doi.org/10.1016/j.jecp.2021.105195

Marzocchi, N., Breveglieri, R., Galletti, C., & Fattori, P. (2008). Reaching activity in parietal area v6a of macaque: Eye influence on arm activity or retinocentric coding

of reaching movements? *European Journal of Neuroscience*, *27*(3), 775–789. https://doi.org/10.1111/j.1460-9568.2008.06021.x

A method of measuring eye movemnent using a scieral search coil in a magnetic field. (1963). *IEEE Transactions on Bio-Medical Electronics*, *10*(4), 137–145. https://doi.org/10.1109/tbmel.1963.4322822

Mooshagian, E., Holmes, C. D., & Snyder, L. H. (2021a). Local field potentials in the parietal reach region reveal mechanisms of Bimanual Coordination. *Nature Communications*, *12*(1). https://doi.org/10.1038/s41467-021-22701-3

Mooshagian, E., Holmes, C. D., & Snyder, L. H. (2021b). Local field potentials in the parietal reach region reveal mechanisms of Bimanual Coordination. *Nature Communications*, *12*(1). https://doi.org/10.1038/s41467-021-22701-3

Mooshagian, E., & Snyder, L. H. (2026). Planning, coordination, and communication: The posterior parietal cortex in eye–hand control. Annual Review of Vision Science. https://doi.org/10.1146/annurev-vision-101922-040813

Moraresku, S., & Vlcek, K. (2020). The use of egocentric and allocentric reference frames in static and dynamic conditions in humans. Physiological Research, 787–801. https://doi.org/10.33549/physiolres.934528

Musa, L., Yan, X., & Crawford, J. D. (2024). Instruction alters the influence of allocentric landmarks in a reach task. *Journal of Vision*, *24*(7), 17. https://doi.org/10.1167/jov.24.7.17

Neggers, S. F. W., Van der Lubbe, R. H. J., Ramsey, N. F., & Postma, A. (2006). Interactions between ego- and allocentric neuronal representations of space. *NeuroImage*, *31*(1), 320–331. https://doi.org/10.1016/j.neuroimage.2005.12.028

Nougaret, S., López-Galdo, L., Caytan, E., Poitreau, J., Barthélemy, F. V., & Kilavik, B. E. (2024). Low and high beta rhythms have different motor cortical sources and

distinct roles in movement control and spatiotemporal attention. *PLOS Biology*, *22*(6). https://doi.org/10.1371/journal.pbio.3002670

Pasqualotto, A., Spiller, M. J., Jansari, A. S., & Proulx, M. J. (2013). Visual experience facilitates allocentric spatial representation. *Behavioural Brain Research*, *236*, 175–179. https://doi.org/10.1016/j.bbr.2012.08.042

Paxinos, G., & Petrides, M. (2024). *The Rhesus Monkey Brain in Stereotaxic Coordinates*. Academic Press.

Pesaran, B., Pezaris, J. S., Sahani, M., Mitra, P. P., & Andersen, R. A. (2002). Temporal structure in neuronal activity during working memory in macaque parietal cortex. *Nature Neuroscience*, *5*(8), 805–811. https://doi.org/10.1038/nn890

Pesaran, B., Nelson, M. J., & Andersen, R. A. (2006). Dorsal premotor neurons encode the relative position of the hand, eye, and goal during reach planning. Neuron, 51(1), 125–134. https://doi.org/10.1016/j.neuron.2006.05.025

Popovych S, Rosjat N, Toth TI, Wang BA, Liu L, Abdollahi RO, Viswanathan S, Grefkes C, Fink GR, Daun S (2016) Movement-related phase locking in the delta-theta frequency band. Neuroimage 139:439–449. https://doi.org/10.1016/j.neuroimage.2016.06.052

Reinshagen, A. (2024). Grid cells: The missing link in understanding Parkinson's disease? Frontiers in Neuroscience, 18. https://doi.org/10.3389/fnins.2024.1276714

Roitman, J. D., & Shadlen, M. N. (2002). Response of neurons in the lateral intraparietal area during a combined visual discrimination reaction time task. *The Journal of Neuroscience*, *22*(21), 9475–9489. https://doi.org/10.1523/jneurosci.22-21-09475.2002

Saleh M, Reimer J, Penn R, Ojakangas CL, Hatsopoulos NG (2010) Fast and slow oscillations in human primary motor cortex predict oncoming behaviorally relevant cues. Neuron 65:461–471. https://doi.org/10.1016/j.neuron.2010.02.001

Scherberger, H., Jarvis, M. R., & Andersen, R. A. (2005). Cortical local field potential encodes movement intentions in the posterior parietal cortex. *Neuron*, *46*(2), 347–354. https://doi.org/10.1016/j.neuron.2005.03.004

Schütz, A., Bharmauria, V., Yan, X. et al. Integration of landmark and saccade target signals in macaque frontal cortex visual responses. Commun Biol 6, 938 (2023). https://doi.org/10.1038/s42003-023-05291-2

Schütz, I., Henriques, D. Y. P., & Fiehler, K. (2013). Gaze-centered spatial updating in delayed reaching even in the presence of landmarks. *Vision Research*, *87*, 46–52. https://doi.org/10.1016/j.visres.2013.06.001

Seo, S., Bharmauria, V., Schütz, A., Yan, X., Wang, H., & Crawford, J. D. (2024). Multiunit frontal eye field activity codes the visuomotor transformation, but not gaze prediction or retrospective target memory, in a delayed saccade task. *Eneuro*, *11*(8). https://doi.org/10.1523/eneuro.0413-23.2024

Sheth, B. R., & Shimojo, S. (2004). Extrinsic cues suppress the encoding of intrinsic cues. *Journal of Cognitive Neuroscience*, *16*(2), 339–350. https://doi.org/10.1162/089892904322984616

Simons, D. J., & Wang, R. F. (1998). Perceiving real-world viewpoint changes. *Psychological Science*, *9*(4), 315–320. https://doi.org/10.1111/1467-9280.00062

Smith, M. A., Majaj, N. J., & Movshon, J. A. (2005). Dynamics of motion signaling by neurons in Macaque Area MT. *Nature Neuroscience*, *8*(2), 220–228. https://doi.org/10.1038/nn1382

Snyder, L. H., Batista, A. P., & Andersen, R. A. (1997). Coding of intention in the posterior parietal cortex. *Nature*, *386*(6621), 167–170. https://doi.org/10.1038/386167a0

Stanton, G. B., Bruce, C. J., & Goldberg, M. E. (1995). Topography of projections to posterior cortical areas from the macaque frontal eye fields. *Journal of Comparative Neurology*, *353*(2), 291–305. https://doi.org/10.1002/cne.903530210

Stetson, C., & Andersen, R. A. (2014). The parietal reach region selectively anti-synchronizes with dorsal premotor cortex during planning. *The Journal of Neuroscience*, *34*(36), 11948–11958. https://doi.org/10.1523/jneurosci.0097-14.2014

Taghizadeh, B., Fortmann, O., & Gail, A. (2024). Position- and scale-invariant object-centered spatial localization in monkey frontoparietal cortex dynamically adapts to cognitive demand. *Nature Communications*, *15*(1). https://doi.org/10.1038/s41467-024-47554-4

Tsao, D. Y., Freiwald, W. A., Tootell, R. B., & Livingstone, M. S. (2006). A cortical region consisting entirely of face-selective cells. *Science*, *311*(5761), 670–674. https://doi.org/10.1126/science.1119983

Wang, J., Du, X., Yao, S., Li, L., Tanigawa, H., Zhang, X., & Roe, A. W. (2024). Mesoscale organization of ventral and dorsal visual pathways in macaque monkey revealed by 7T fmri. *Progress in Neurobiology*, *234*, 102584. https://doi.org/10.1016/j.pneurobio.2024.102584

Westwood, D. A., Heath, M., & Roy, E. A. (2001). The accuracy of reaching movements in brief delay conditions. *Canadian Journal of Experimental Psychology / Revue Canadienne de Psychologie Expérimentale*, *55*(4), 304–310. https://doi.org/10.1037/h0087377

Whitwell, J. L., Jones, D. T., Duffy, J. R., Strand, E. A., Machulda, M. M., Przybelski, S. A., Vemuri, P., Gregg, B. E., Gunter, J. L., Senjem, M. L., Petersen, R. C., Jack, C. R., & Josephs, K. A. (2015). Working memory and language network dysfunctions in logopenic aphasia: A task-free fMRI comparison with Alzheimer's dementia. Neurobiology of Aging, 36(3), 1245–1252. https://doi.org/10.1016/j.neurobiolaging.2014.12.013

Wood, R. A., Moodley, K. K., Lever, C., Minati, L., & Chan, D. (2016). Allocentric spatial memory testing predicts conversion from mild cognitive impairment to dementia: An

initial proof-of-concept study. Frontiers in Neurology, 7. https://doi.org/10.3389/fneur.2016.00215

Yttri, E. A., Wang, C., Liu, Y., & Snyder, L. H. (2014). The parietal reach region is limb specific and not involved in eye-hand coordination. *Journal of Neurophysiology*, *111*(3), 520–532. https://doi.org/10.1152/jn.00058.2013

APPENDICES

Appendix A: Author Contributions

I contributed to the data collection, analysis, interpretation, and I wrote this paper. Dr. Nácher and Jennifer Lin collected the LFP data, and Saihong Sun and Ashkan Karimi wrote the statistical analysis code. Dr. Crawford contributed to the project design, data interpretation and provided editorial comments.